AIE active acidochromic pyrimidine functionalized two-in-one fluorescent probe for selective relay detection of Al^{3+}/Zn^{2+} and PPi with various detection applications

Ottoor Anitha,[a] Janardhanan Aiswarya,[a] Thangaraj Thiruppathiraja,[b] Senthilkumar Lakshmipathi,[b] Jan Grzegorz Małecki,[c] Balasubramanian Murugesapandian*[a]

[a]Department of Chemistry, Bharathiar University, Coimbatore, 641046, Tamil Nadu, India. E-mail: mpandian@gmail.com; bmurugesapandian@buc.edu.in Fax: +91-422-2422387; Tel: +91-422-2428312.

[b]Department of Physics, Bharathiar University, Coimbatore, 641046, Tamil Nadu, India.

[c] Institute of Chemistry, University of Silesia, Szkolna 9, 40-006 Katowice, Poland

Table of contents

Preparation of stock solutions for spectroscopic experiments

Stock solutions of 1 × 10^{-3} N concentration were prepared for **HSAL** DMF solvent. Likewise, 1 × 10^{-3} N of metal salt stock solutions were prepared in methanol medium. For performing the spectroscopic experiments, DMF- Tris HCl buffer solution with pH=7.4 is utilized for the studies.

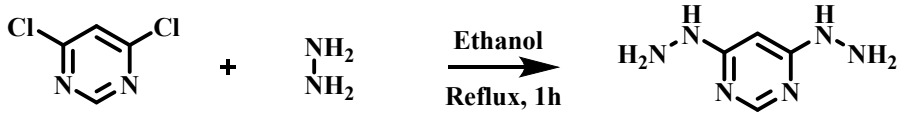

Scheme S1. Synthesis of *4,6*-dihydrazinopyrimidine.

Stock solution preparations for photophysical studies

1×10^{-3} M stock solutions of **HSAL** in DMF. The absorbance, and emission spectroscopic measurements were carried out by diluting the solution into 1 × 10^{-5} M

concentrations. 500 μL of 1×10^{-3} M stock solutions of the compound in DMF are used for preparing 5 mL, 1×10^{-4} M solutions in separate vials for aggregation as well as for DLS measurements by varying water fractions from 0-99%. Ultrapure distilled water was used for aggregation and DLS studies. 40 μL probe solution was diluted to 2.5 mL of DMF-Tris-HCl (6:4, v/v, pH 7.2) to make the final concentration of 16 μM. 1×10^{-3} M cationic and anionic solutions were prepared in in distilled water. UV-Vis and emission experiments were carried out between the probe and cations by following certain required concentrations.

Fluorescence quantum yield measurements

Fluorescence quantum yield measurements for **HYPY-DESAL** in various solvents have been estimated by using quinine sulphate dye as a standard (Φ_F = 0.546) in 0.5 M H_2SO_4 solution using the formula:

$$\Phi_f = \Phi_s \times \left(\frac{I_x}{I_s}\right) \times \left(\frac{A_s}{A_x}\right) \times \left(\frac{\eta_x}{\eta_s}\right)^2$$

where ϕ_f and ϕ_s corresponds to the fluorescence quantum yield of sample and standard respectively. A_x and A_s represents integrated area under the emission spectra of sample and standard and η is the refractive index of the solvent used. I_x and I_s absorption optical density value for sample and standard.

Calculation of the binding stoichiometry and association constant

The binding stoichiometry of the metal ion to the probe **HSAL** was determined by using the mole ratio method of Job plot experiments.[1]The association constant was determined by following the equation.[2]

$$(x) = (a + b \times cx^n)/(1 + cx^n)$$

Where, **x** is the concentration of ion, **F(x)** is the intensity, **a** is the intensity of probe without ions, **b** is the intensity at the saturation, **n** is the binding stoichiometry and **c** is the association constant. The association constant of the Al^{3+}/ Zn^{2+} ensemble binding to the PPi was determined from the fluorescence titration data based on the reported Benesi-Hildebrand equation.[3]

$$1/\Delta A \; vs \; 1/[M^+]$$

Calculation of Detection limit

Detection limit was calculated by following the emission titration spectra of HSAL on adding increments of Al^{3+}/ Zn^{2+}. A linear response was obtained on plotting the L.O.D spectra upto the saturation limit and the detection limit of HSAL towards both ions as well as L.O.D of HSAL-Al^{3+} and HSAL-Zn^{2+} ensembles towards PPi was calculated according to the following equation.

$$LOD = 3s/m$$

Where, s is the standard deviation of blank measurements and m is the slope value obtained from the calibration curve.

Extraction of aluminium content from the pharmaceutical tablet

Gelucil tablets were collected and it was finely powdered. The powder was then dissolved in 20 mL of 2N HNO_3 and kept for 8 hours stirring. The solution was then filtered out and the filtrate was diluted with distilled water by making the total volume of the solution up to 100 mL and pH of the diluted extract was then adjusted to 7.2. The prepared solution was then used for the emission titration at ambient temperature.

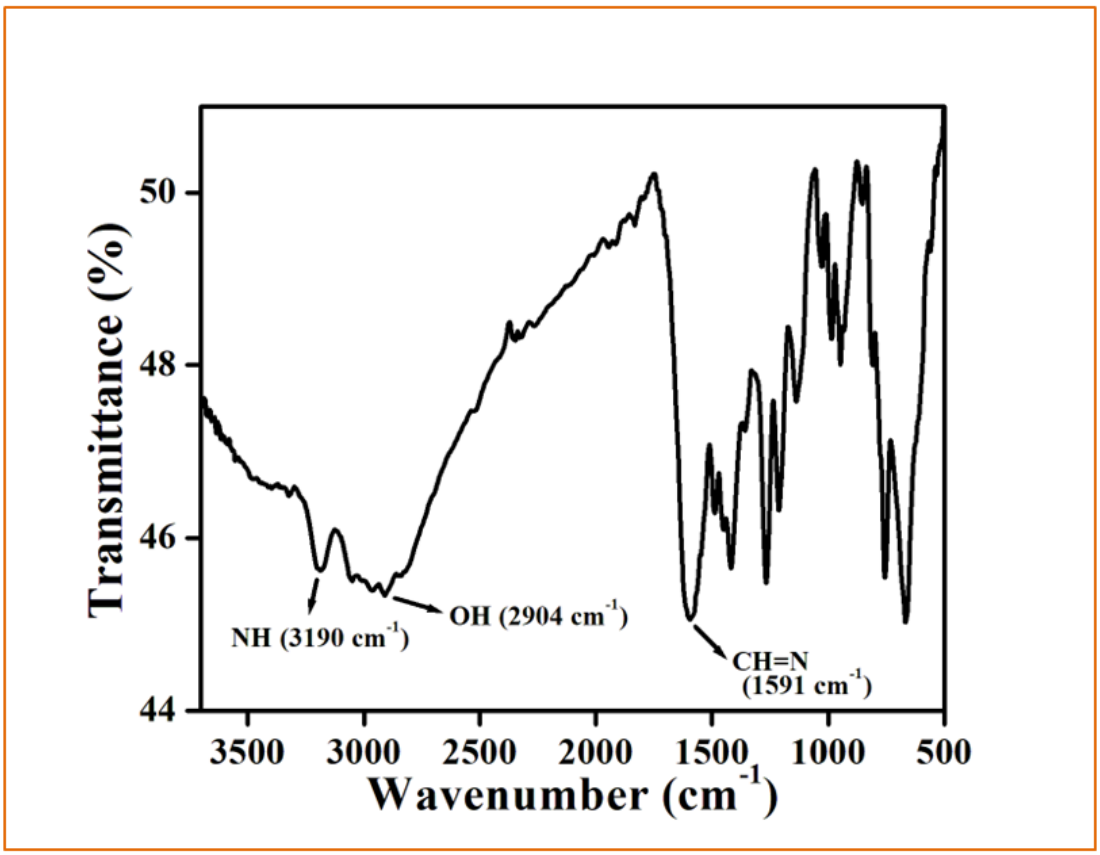

Fig S1. FT-IR spectrum of **HSAL**

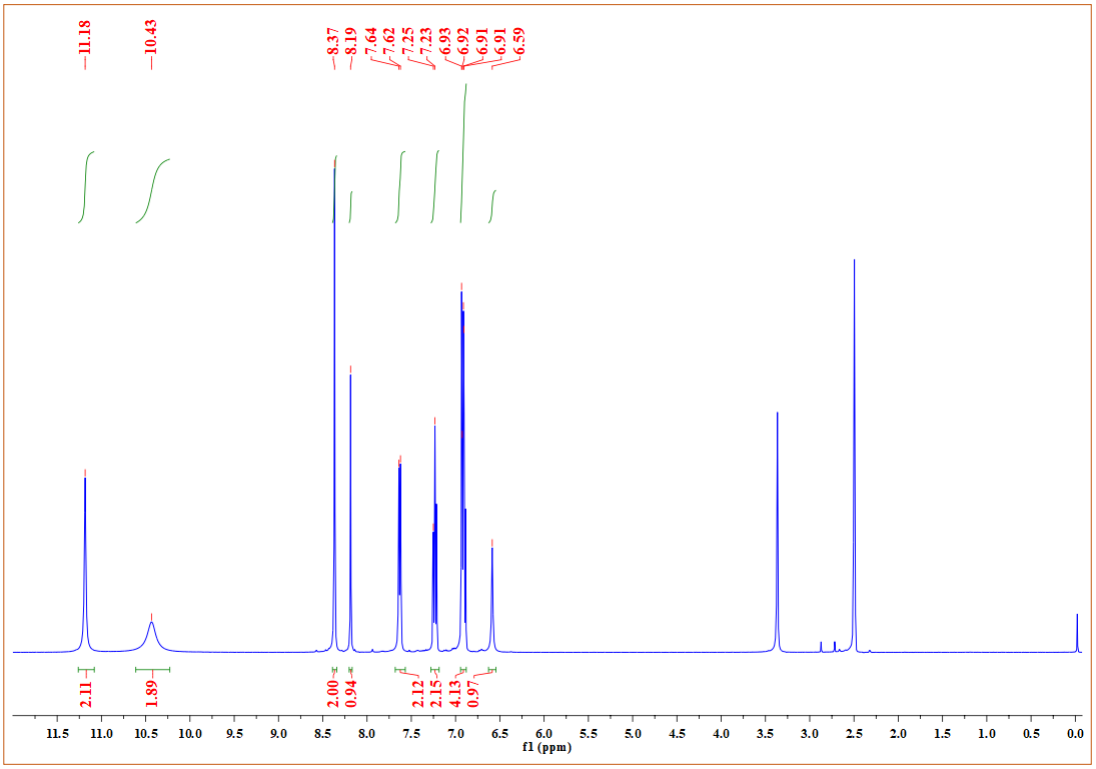

Fig S2. ^{1}H NMR spectrum of **HSAL**.

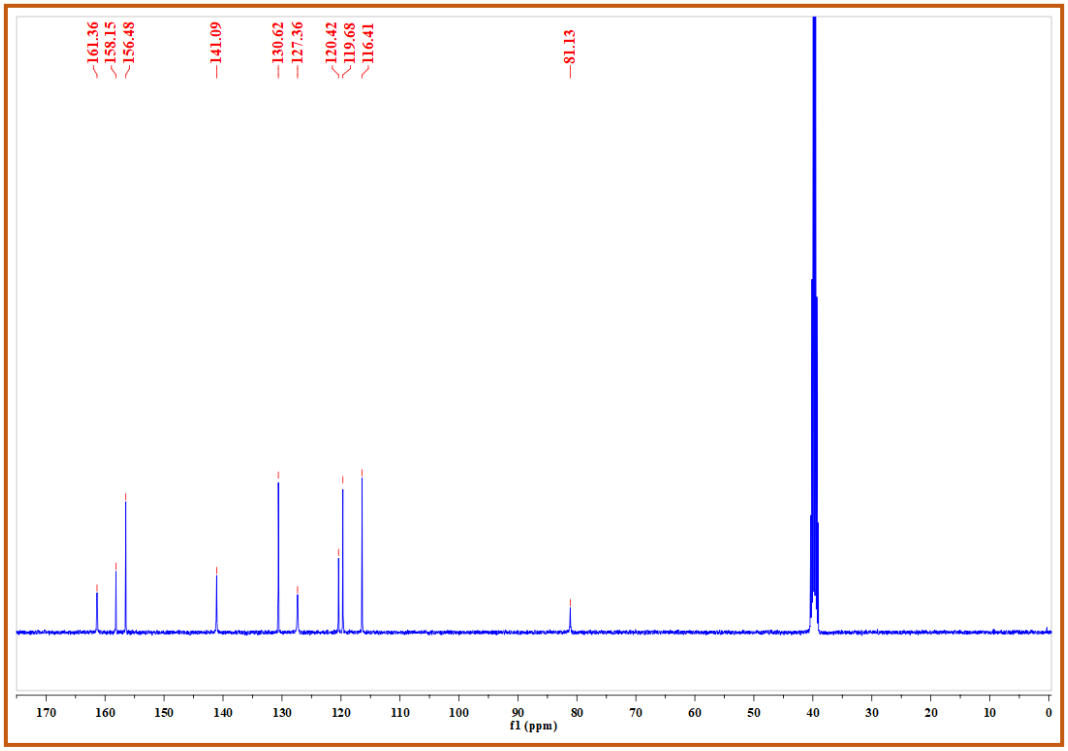

Fig S3. ^{13}C NMR spectrum of **HSAL**.

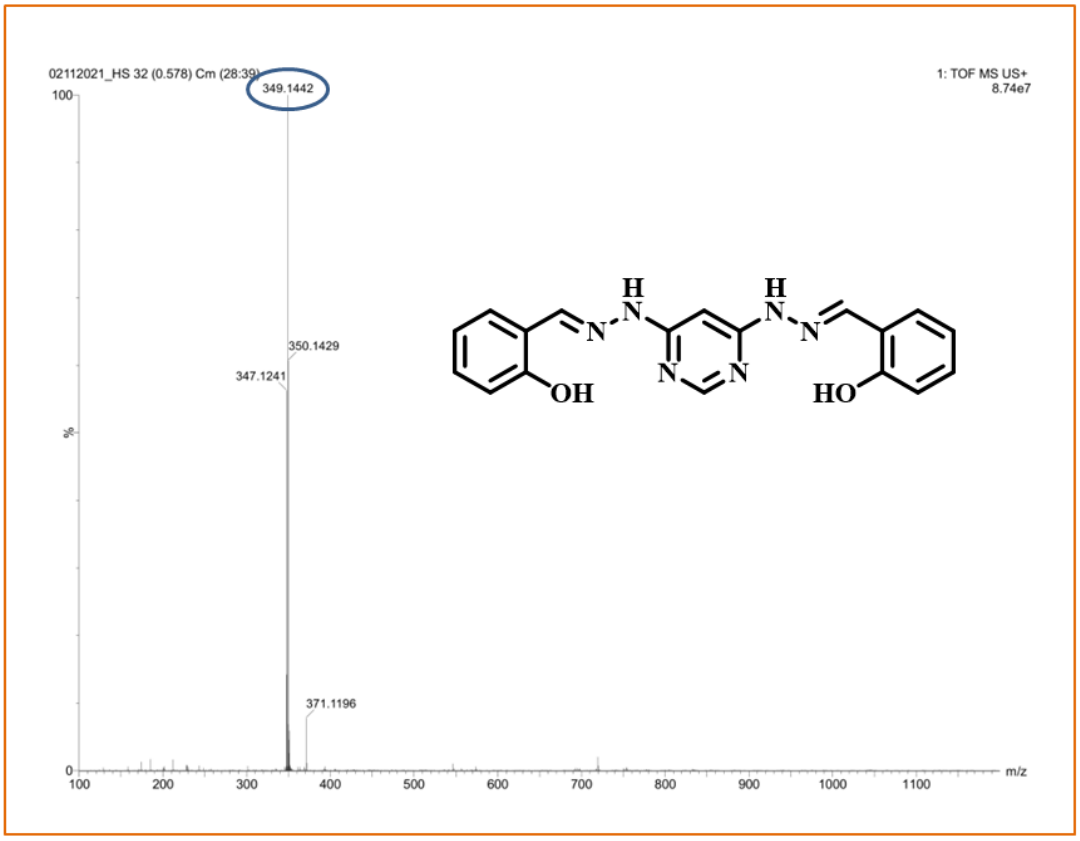

Fig S4. Mass spectrum of **HSAL**.

Table S1. Crystal data and structure refinement details of **HSAL**

	HSAL
Formula	$C_{18}H_{16}N_6O_2$
Formula weight	348.37
Temperature (K)	295(2)
Crystal system	orthorhombic
Space group	$P2_12_12_1$
Unit cell dimensions	
a (Å)	9.2582(7)
b (Å)	12.0267(8)
c (Å)	30.804(2)
α (°)	90
β (°)	90
γ (°)	90
V (Å^3)	3429.9(4)
Z	8
Density(calcd) (g/cm^3)	1.349
Abs. coeff. (mm^{-1})	0.093
F(000)	1456
Crystal size (mm)	0.27x0.21x0.07
Radiation (Å)	0.71073
θ Min, Max (°)	3.388, 29.475
Data set h, k, l	−12:9, −16:11, −41:42
Tot./ Uniq. Data	14030 / 7383
R (int)	0.0284
N_{ref}, N_{par}	7383, 501
R, wR_2, S	**0.0499, 0.0944, 1.025**

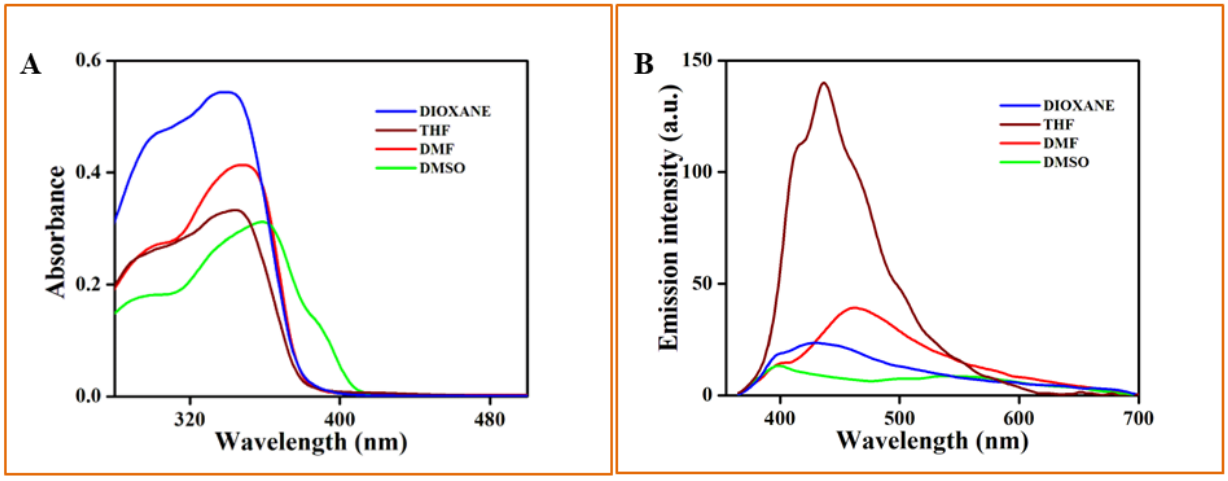

Fig S5. (A) Absorption and (B) Emission spectra (λ_{ex}=355 nm) of **HSAL** (1 × 10^{-5} M) in different solvents.

Frontier molecular orbitals

The frontier molecular orbitals (FMOs) of highest-occupied molecular orbital (HOMO) and lowest-unoccupied molecular orbital (LUMO) energies are calculated. The HOMO-LUMO (E_{H-L}) gap is calculated as the difference between the LUMO and HOMO energies ($E_{HOMO-LUMO}$ gap = $E_{LUMO} - E_{HOMO}$).[4] Generally, the E_{H-L} gap explains the stability and reactivity of the compound structure. Besides the higher E_{H-L} energy gap of a compound indicates higher stability and a lower reactivity while the lower E_{H-L} gap represents the lesser stability with the highest reactivity of a compound. The $E_{HOMO-LUMO}$ gap values are tabulated in **Table S3** and the corresponding E_{H-L} plots as given in **Fig. S6 & S7** (the contour value is 0.04 a.u.). From **Fig. S6 & S7**, the positive and negative values represent the phase of the frontier orbitals colors in which the negative phase indicates blue and the positive as red.[5]

Table S2**.** Photophysical parameters of **HSAL** in various solvents.

Solvents	**λ_{abs} (nm)**	**λ_{em} (nm)**	**Quantum yield (ϕ_F)**	**Molar absorptivity ε_{abs} (M^{-1} cm^{-1})**
THF	300,340	415, 436	0.109	6.5 × 10^4
DIOXANE	300,340	400, 430	0.021	8.7 × 10^4
DMF	300,340	398, 460	0.024	8.5 × 10^4
DMSO	300,360	398, 545	0.038	6.1 × 10^4

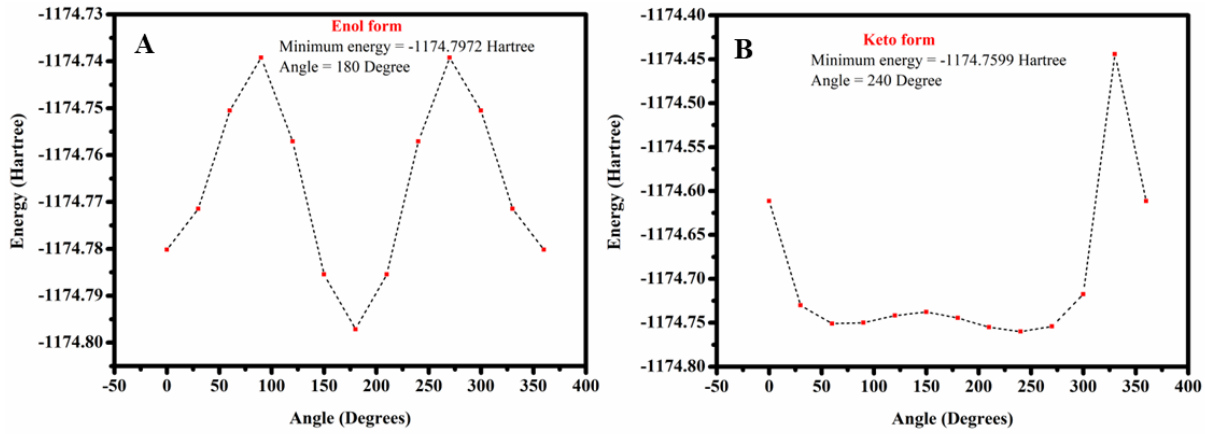

Fig S6. The optimized geometries of various possible conformers of (A) enol form (B) keto form.

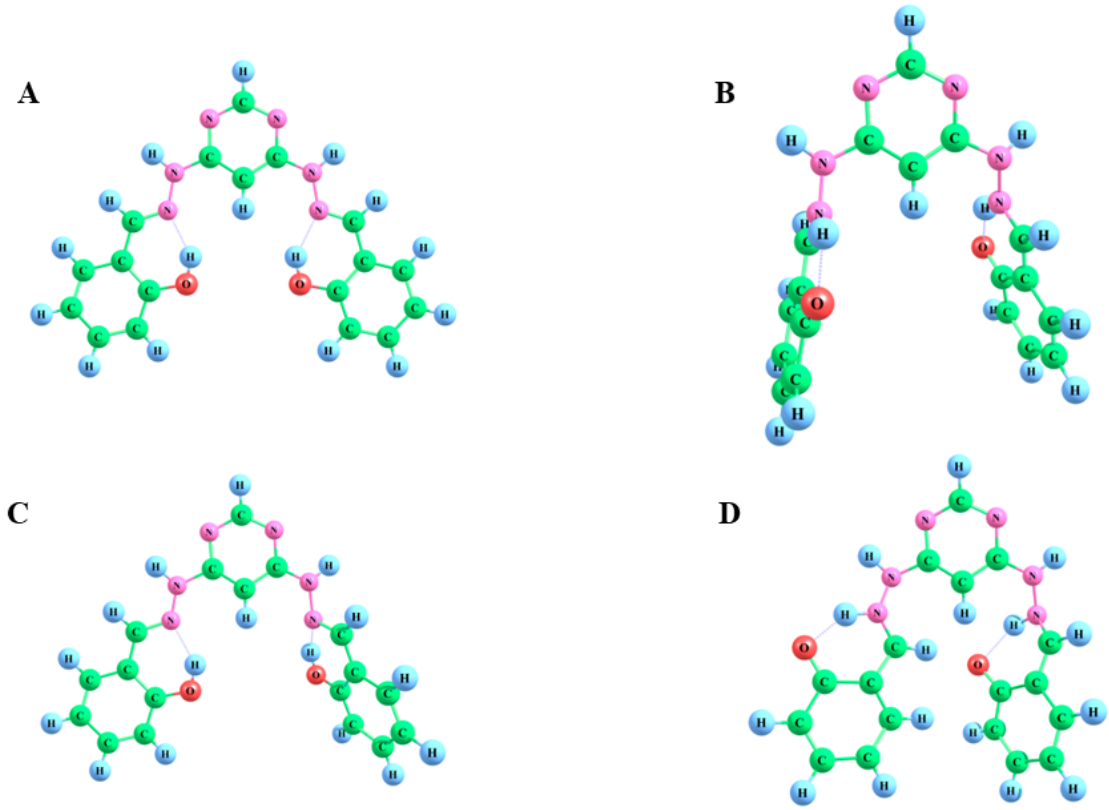

Fig S7. The optimized geometries of Enol and Keto forms of (A & B) ground state and (C&D) excited state.

Table S3. The optimized geometry for the ground state and excited state energy of Enol and Keto form at calculated B3LYP/6-311++G(d,p) level of theory.

Structure	**Ground state energy (in Hartree)**	**Excited state energy (in Hartree)**
Enol	-1174.7972	-1174.6855
Keto	-1174.7599	-1174.6860

Table S4. The HOMO-LUMO gap for ground and excited state energies of Enol and Keto form.

Structure	**Ground state energy / eV**			**Excited state energy / eV**		
	HOMO	**LUMO**	**HOMO-LUMO gap**	**HOMO**	**LUMO**	**HOMO-LUMO gap**
Enol	-6.00	-1.93	4.07	-5.46	-2.79	2.67
Keto	-5.96	-2.40	3.56	-4.96	-3.76	1.20

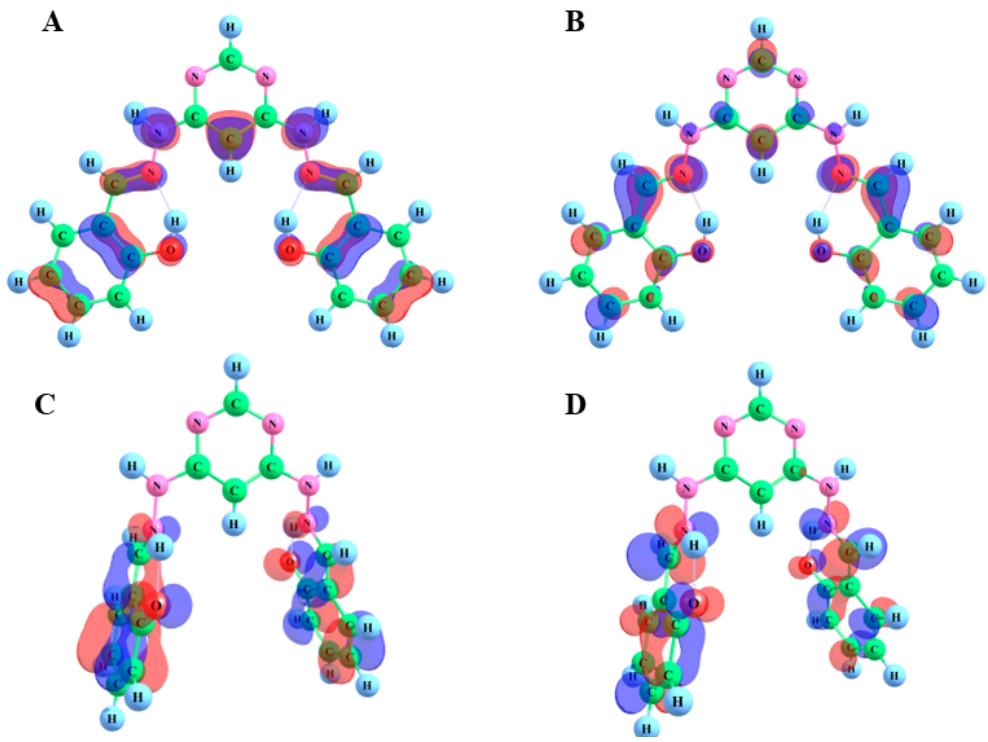

Fig. S8. The HOMO-LUMO plots for ground state energy of (A), (B) Enol form (C), (D) Keto form.

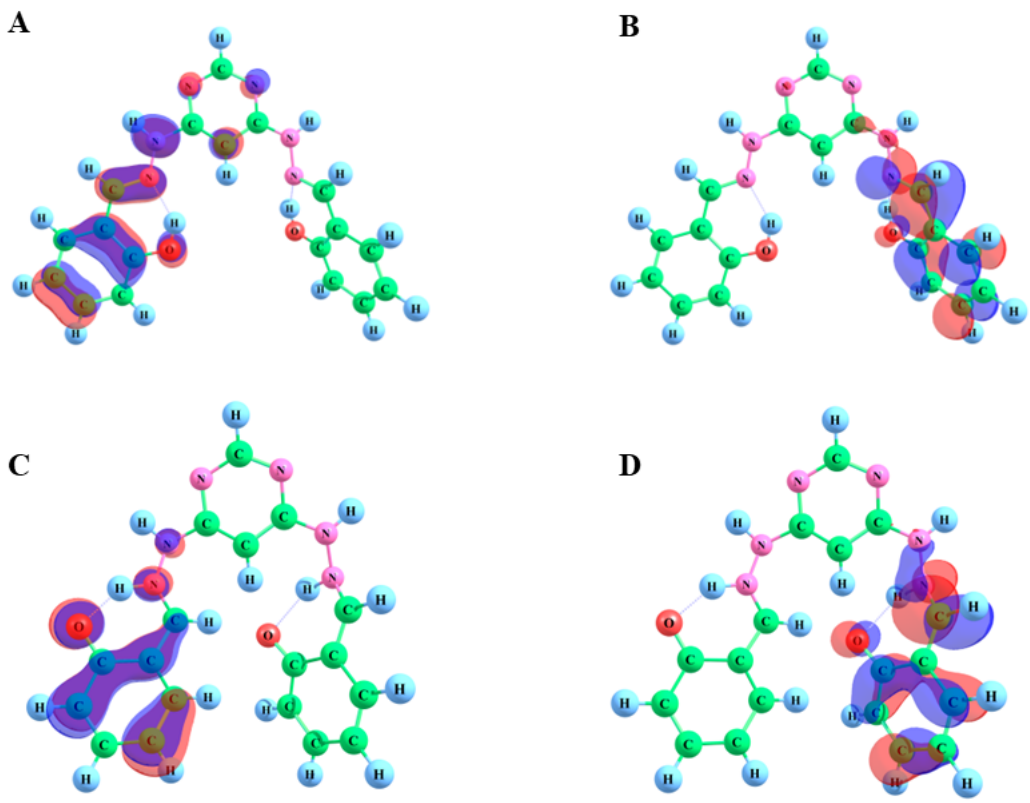

Fig. S9. The HOMO-LUMO plots for excited state energy of (A), (B) Enol form (C), (D) Keto form.

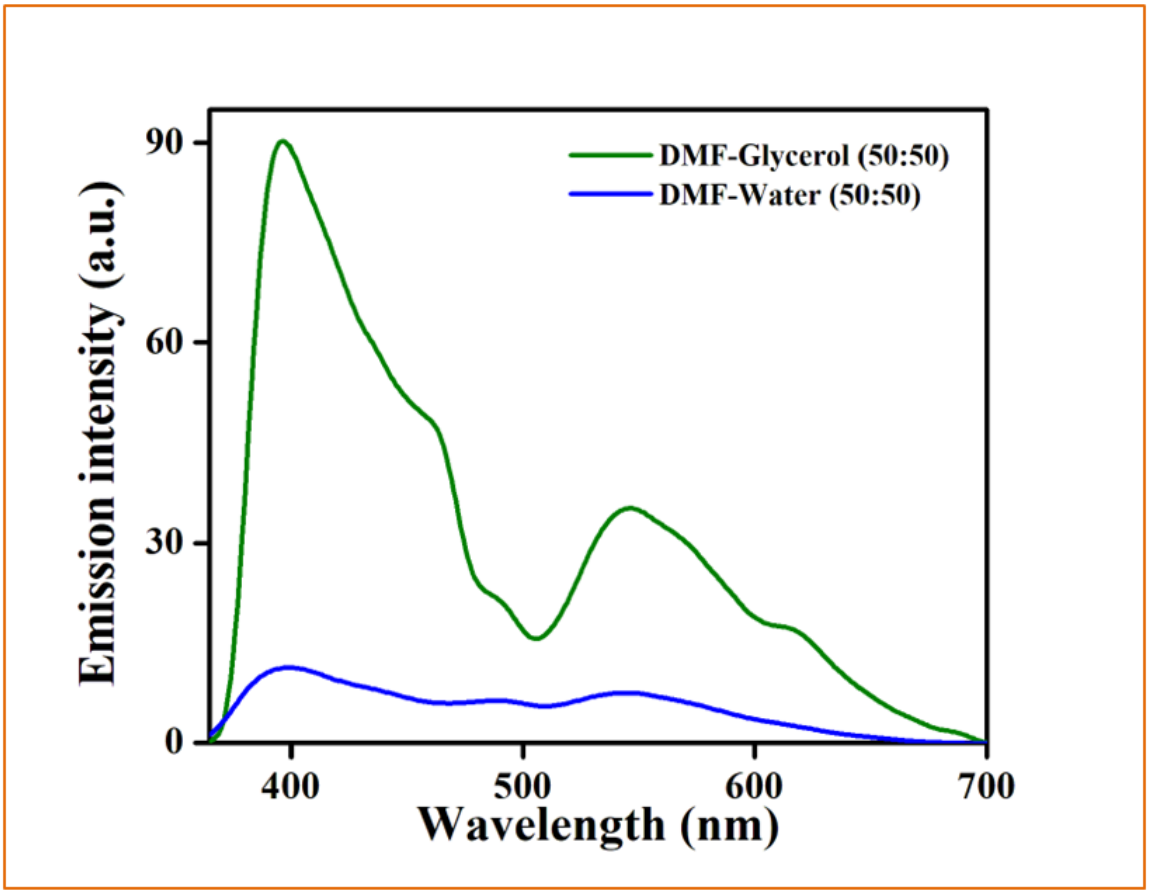

Fig. S10. Fluorescence spectra of **HSAL** in DMF-Water and DMF-Glycerol mixture.

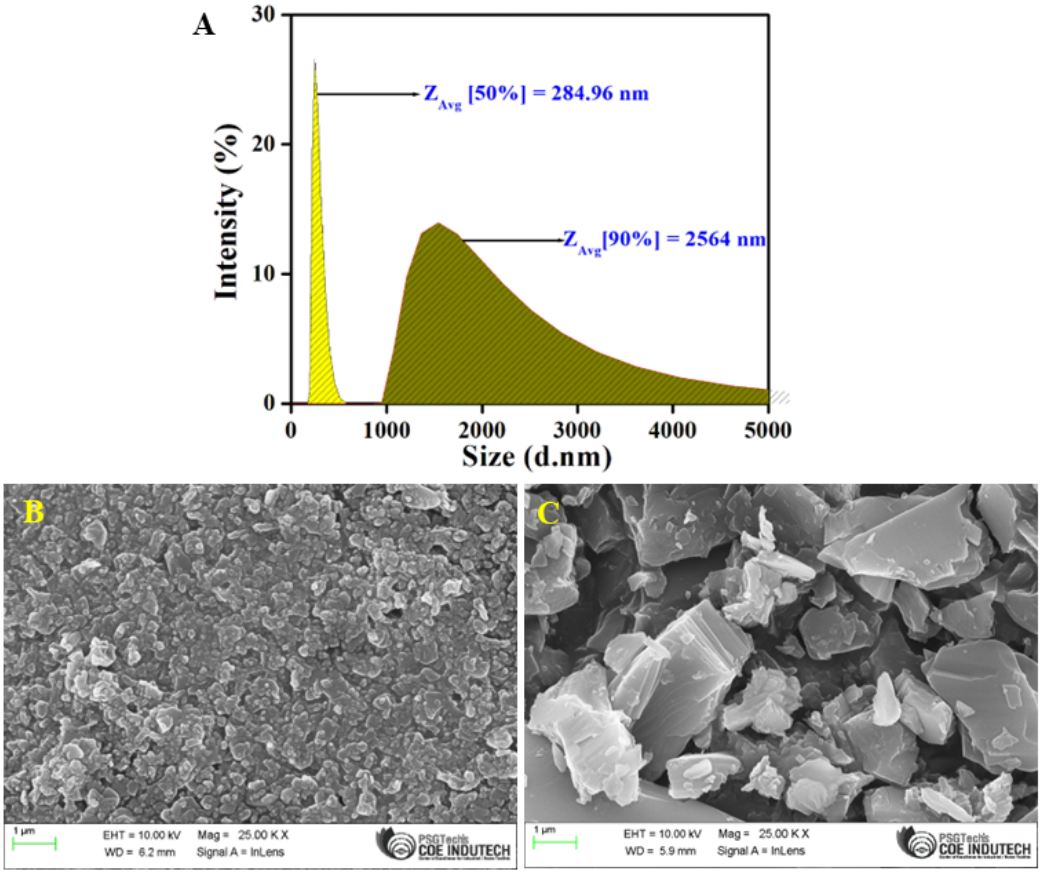

Fig S11. (A) Dynamic light scattering measurement of **HSAL** with particle size distribution at DMF/water mixtures, and Field emission scanning electron microscopy (FESEM) images of **HSAL** at (B) 50% and (C) 90% of water fractions in DMF/water mixtures.

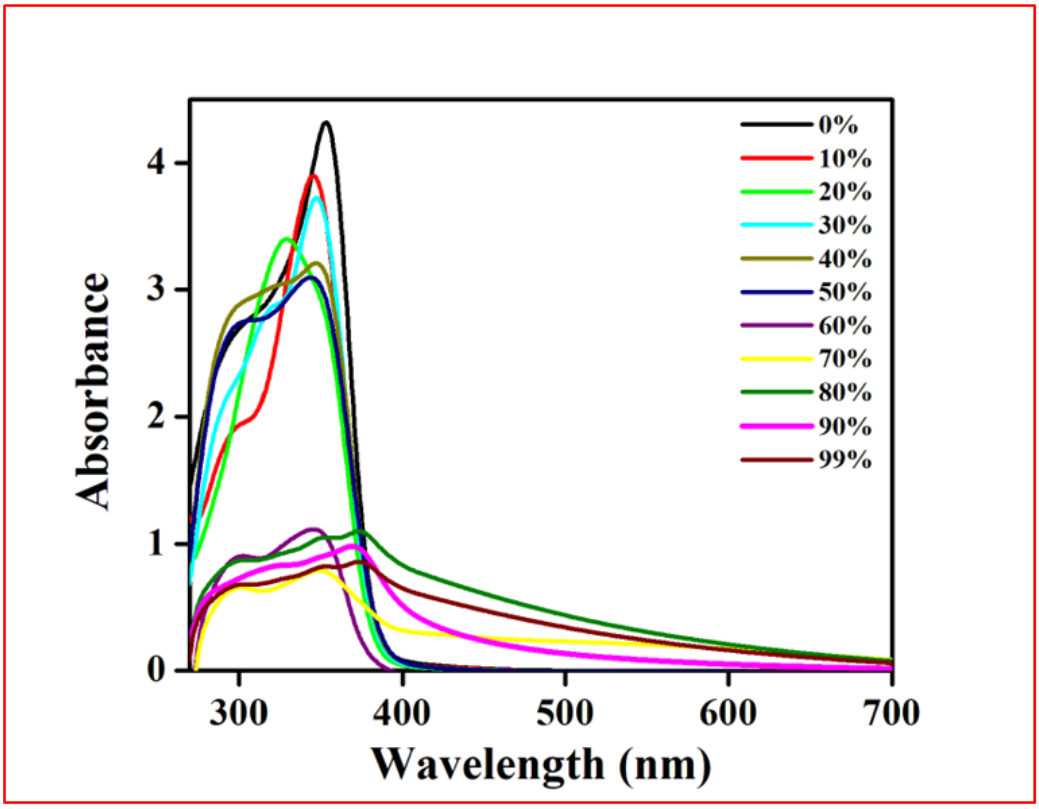

Fig S12. UV-Vis spectra of **HSAL** (100 μM) upon varying water fractions in DMF/water mixture.

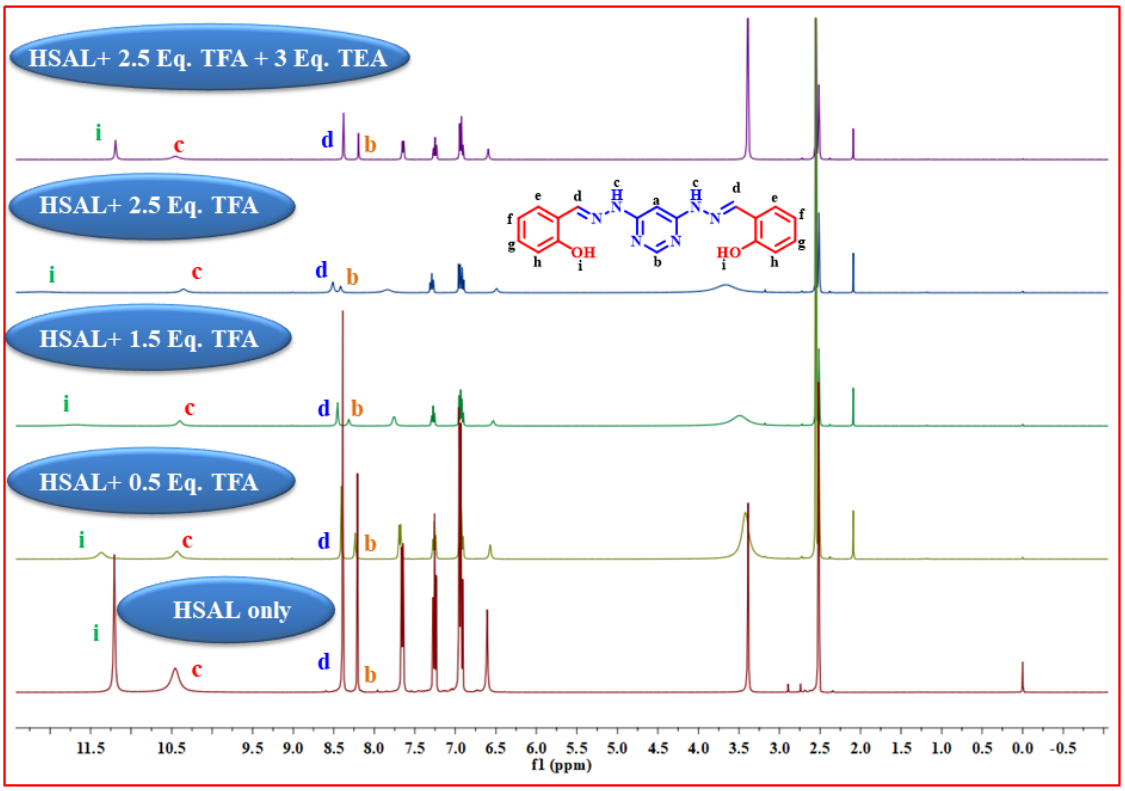

Fig S13. ^{1}H NMR titration experiment on **HSAL** in DMSO-d_6 on successive incremental addition of TFA/TEA.

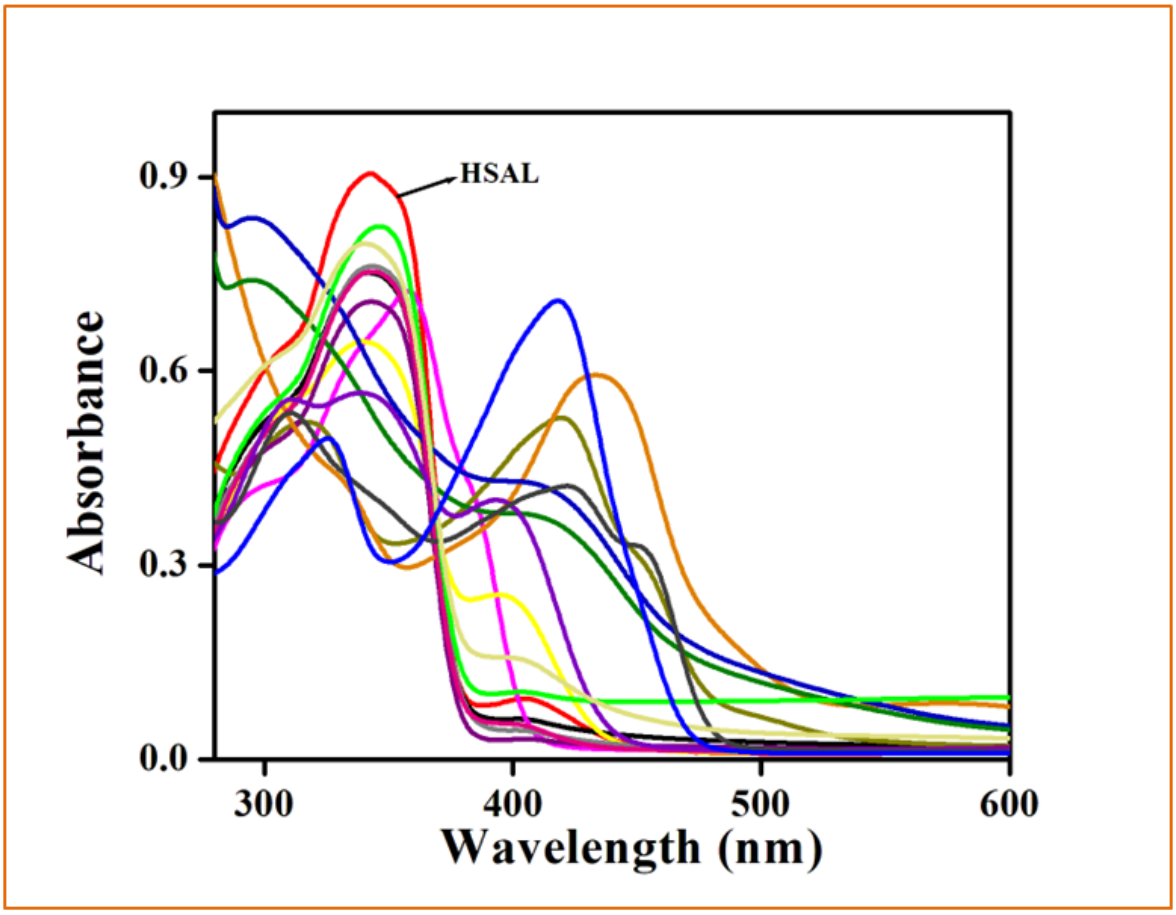

Fig S14. UV-Vis spectra of **HSAL** on adding 10 equivalents of various metal ions in DMF-Tris-HCl buffer solution (10 mM Tris-HCl, 8:2 v/v, pH 7.4).

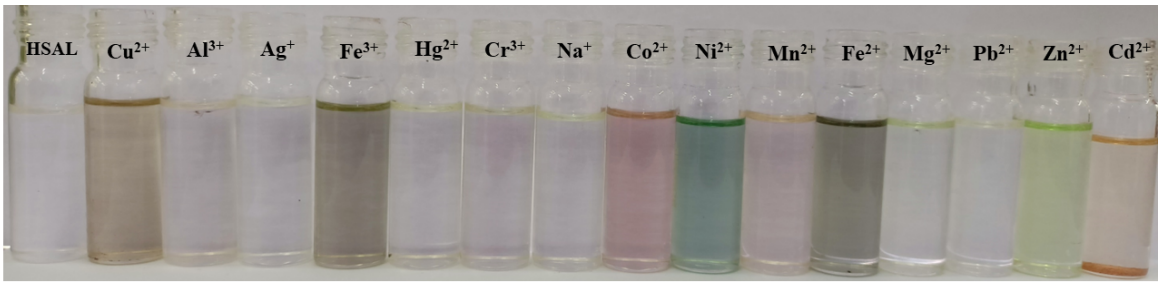

Fig S15. Photographic images of vials containing **HSAL** on adding different metal ions under visible light in DMF-Tris-HCl buffer solution (10 mM Tris-HCl, 8:2 v/v, pH 7.4)

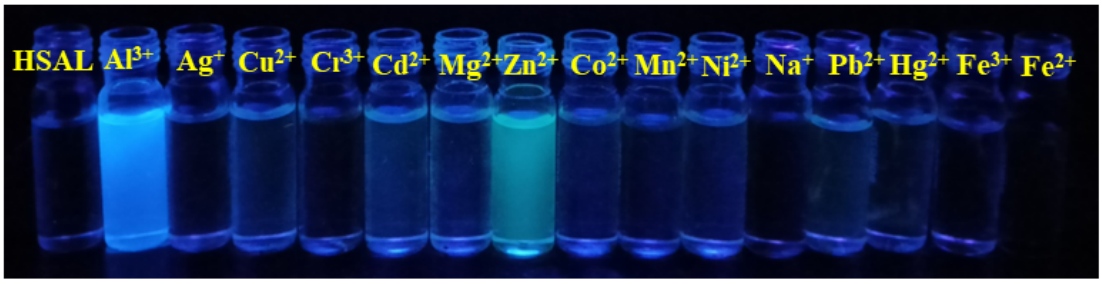

Fig S16. Photographic images of vials containing **HSAL** on adding different metal ions under UV light in DMF-Tris-HCl buffer solution (10 mM Tris-HCl, 8:2 v/v, pH 7.4).

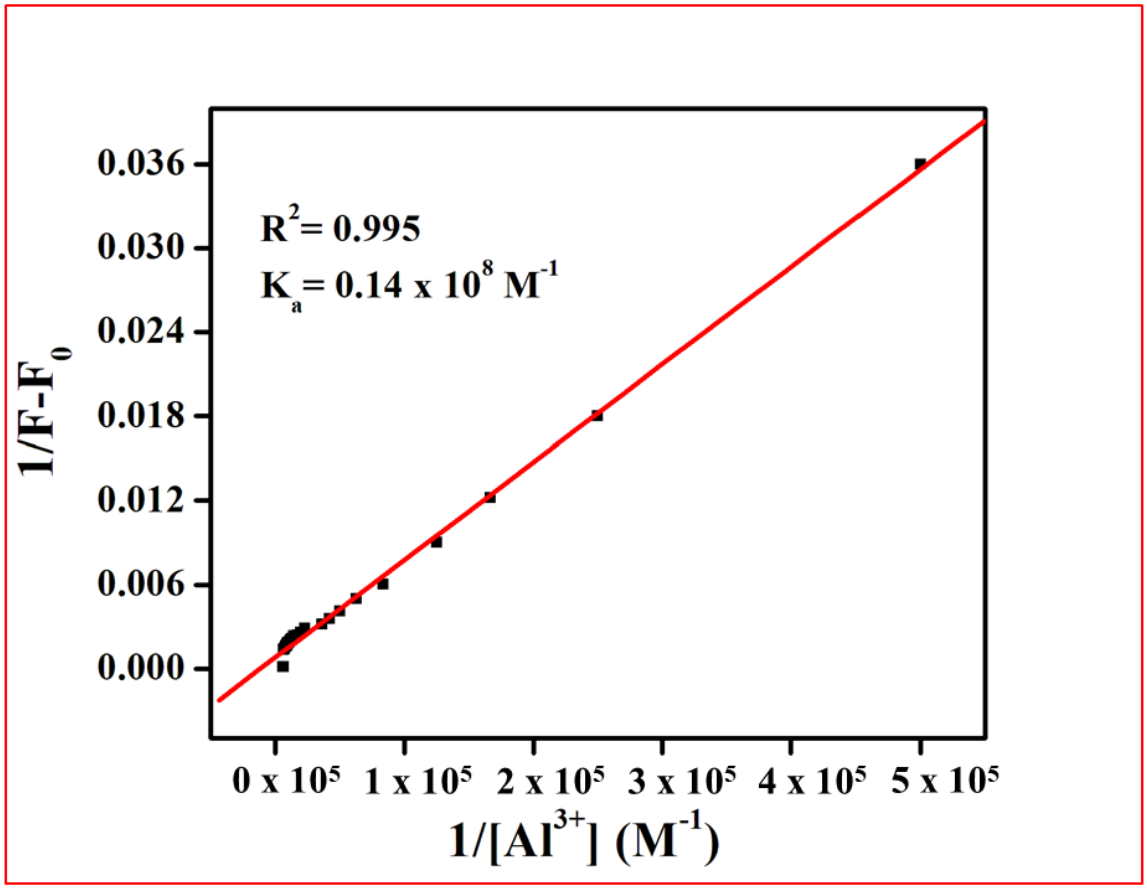

Fig S17. Benesi-Hildebrand plot for the detection of Al^{3+} ion by **HSAL** (0–20 Equiv.).

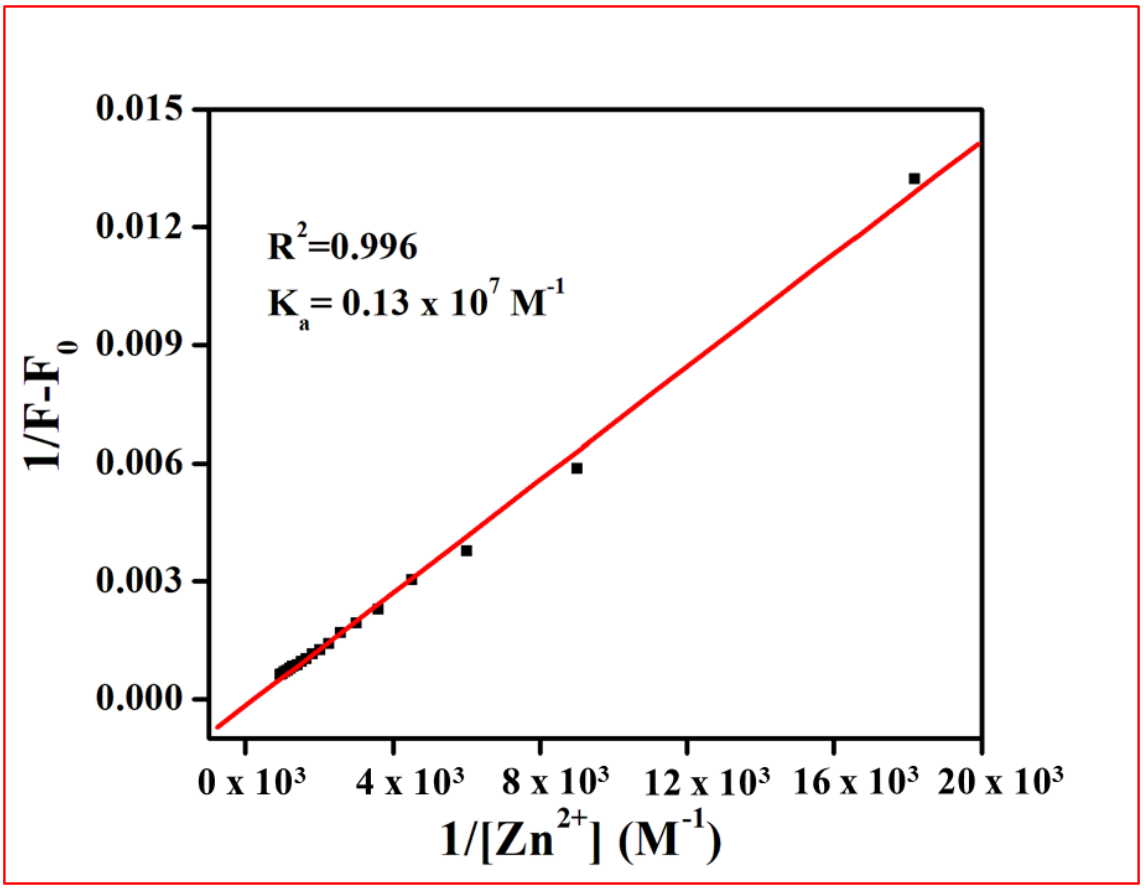

Fig S18. Benesi-Hildebrand plot for the detection of Zn^{2+} ion by **HSAL** (0–22 Equiv.)

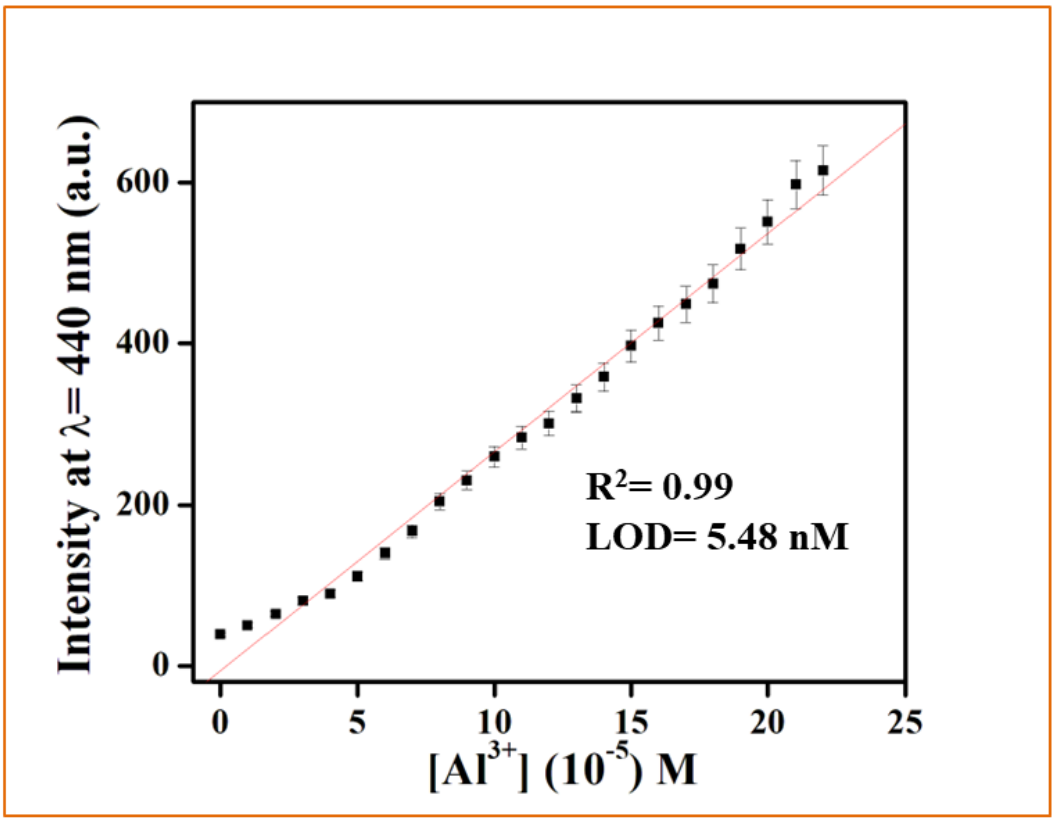

Fig S19. Linear fit curve of **HSAL** with respect to Al^{3+} concentration at 440 nm. Standard deviations are represented by error bar (n=5).

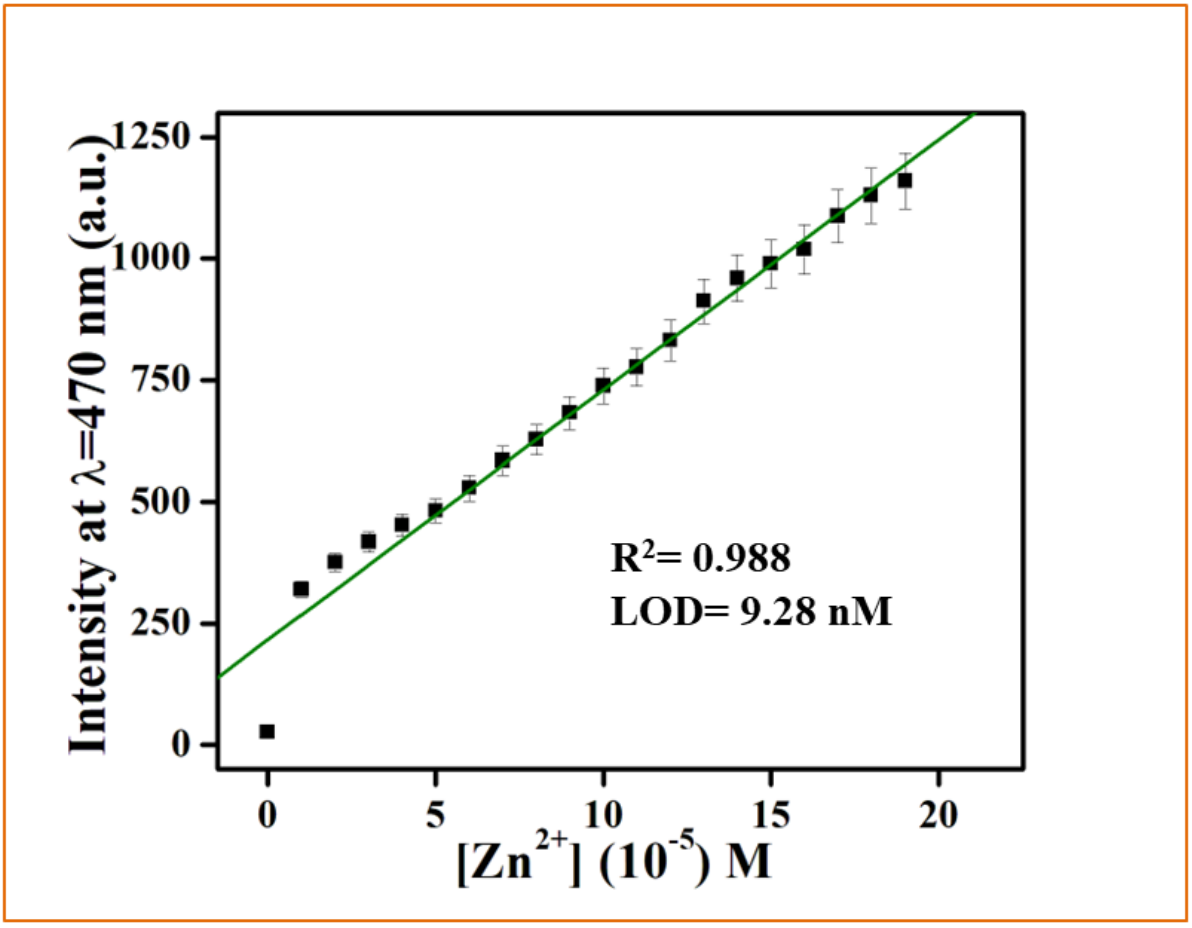

Fig S20. Linear fit curve of **HSAL** with respect to Zn^{2+} concentration at 470 nm. Standard deviations are represented by error bar (n=5).

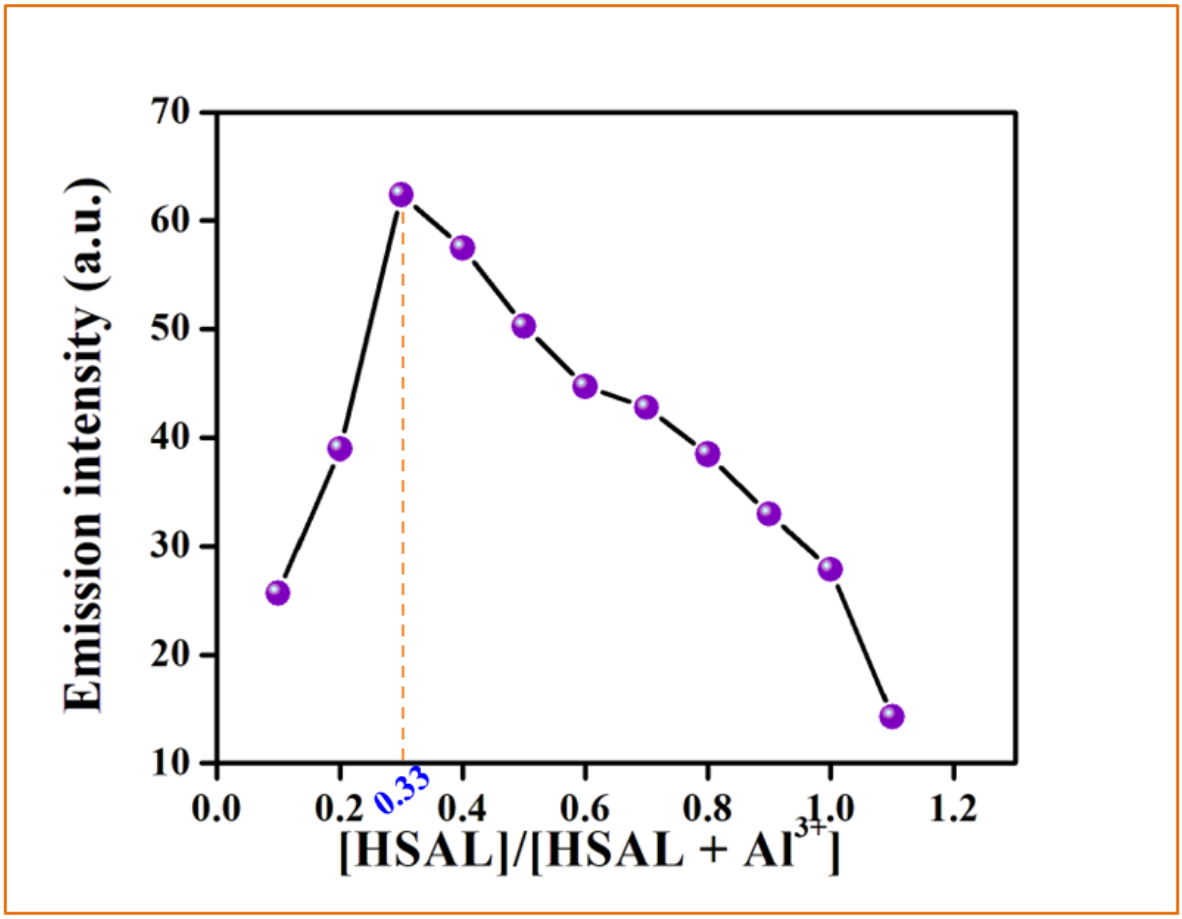

Fig S21. Job's plot of **HSAL** for determining the binding stoichiometry towards Al^{3+} ions at λ= 440 nm.

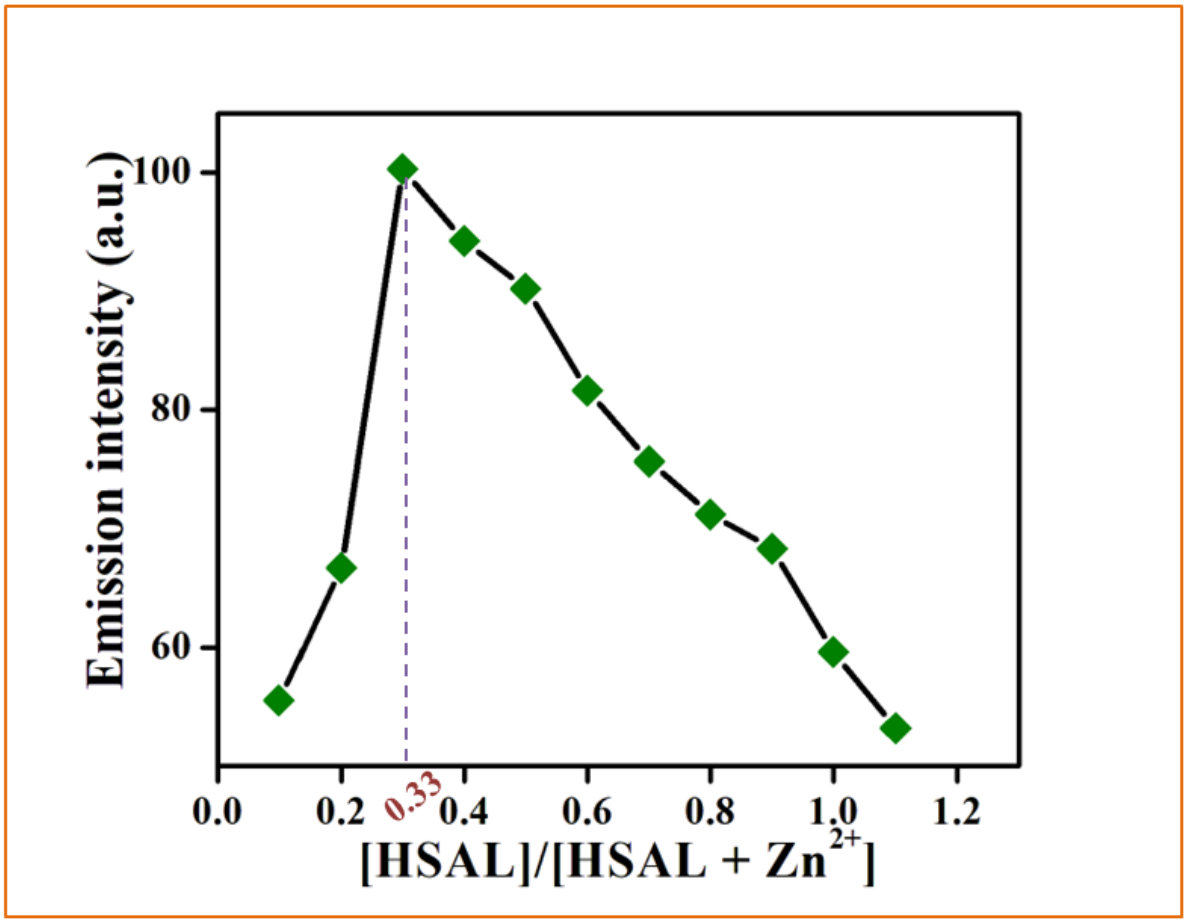

Fig S22. Job's plot of **HSAL** for determining the binding stoichiometry towards Zn^{2+} ions at λ= 470 nm.

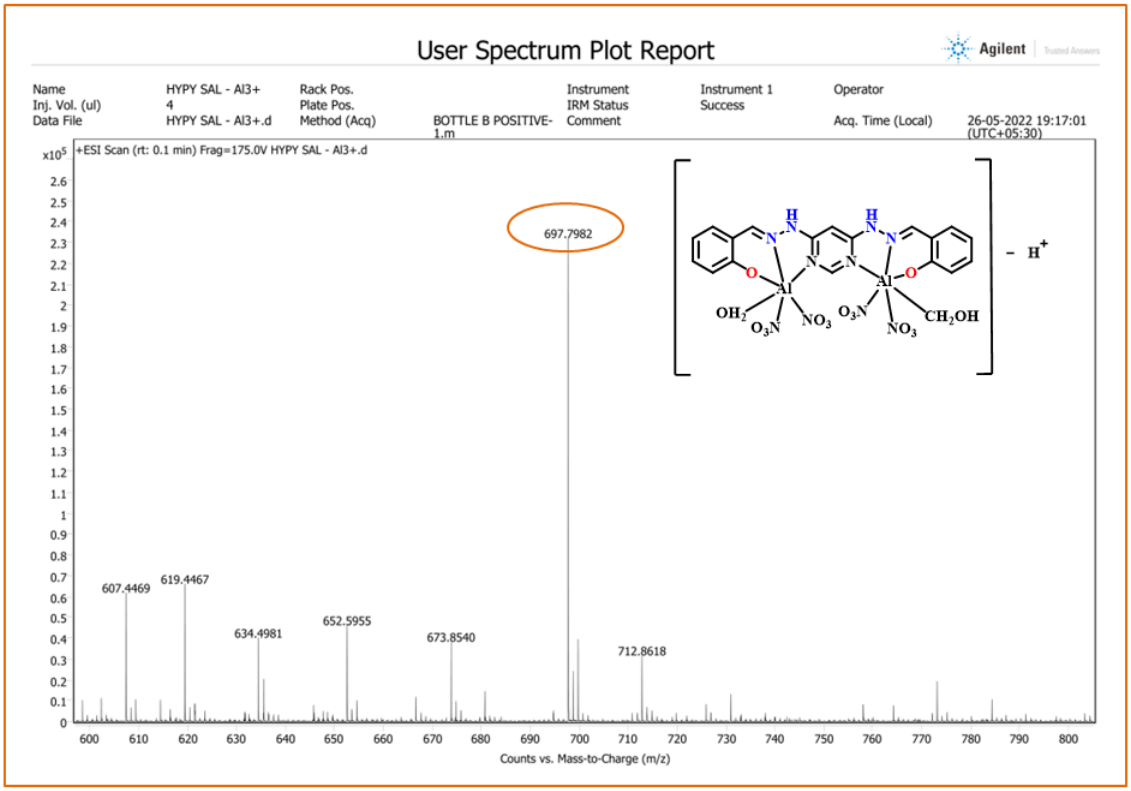

Fig S23. Mass spectrum of HSAL-Al^{3+}

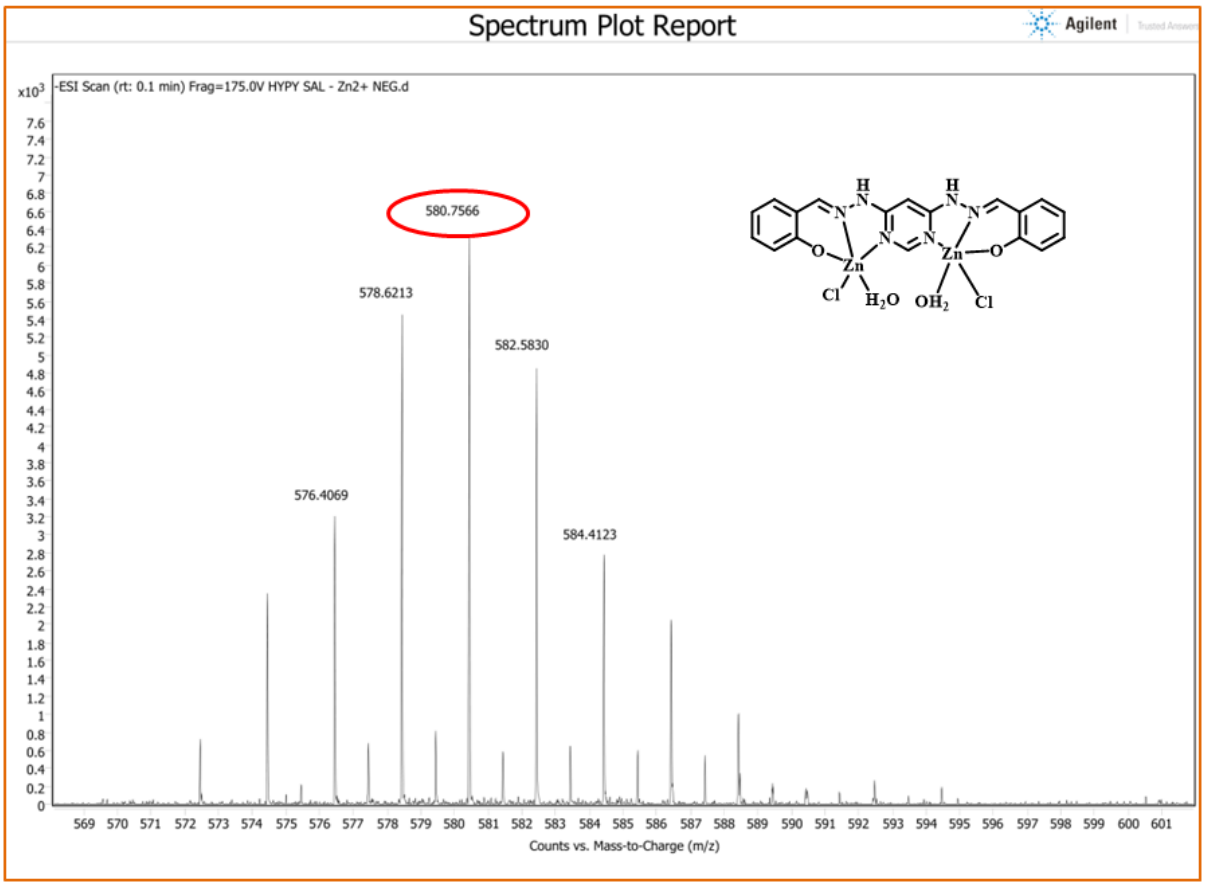

Fig S24. Mass spectrum of HSAL- Zn^{2+}.

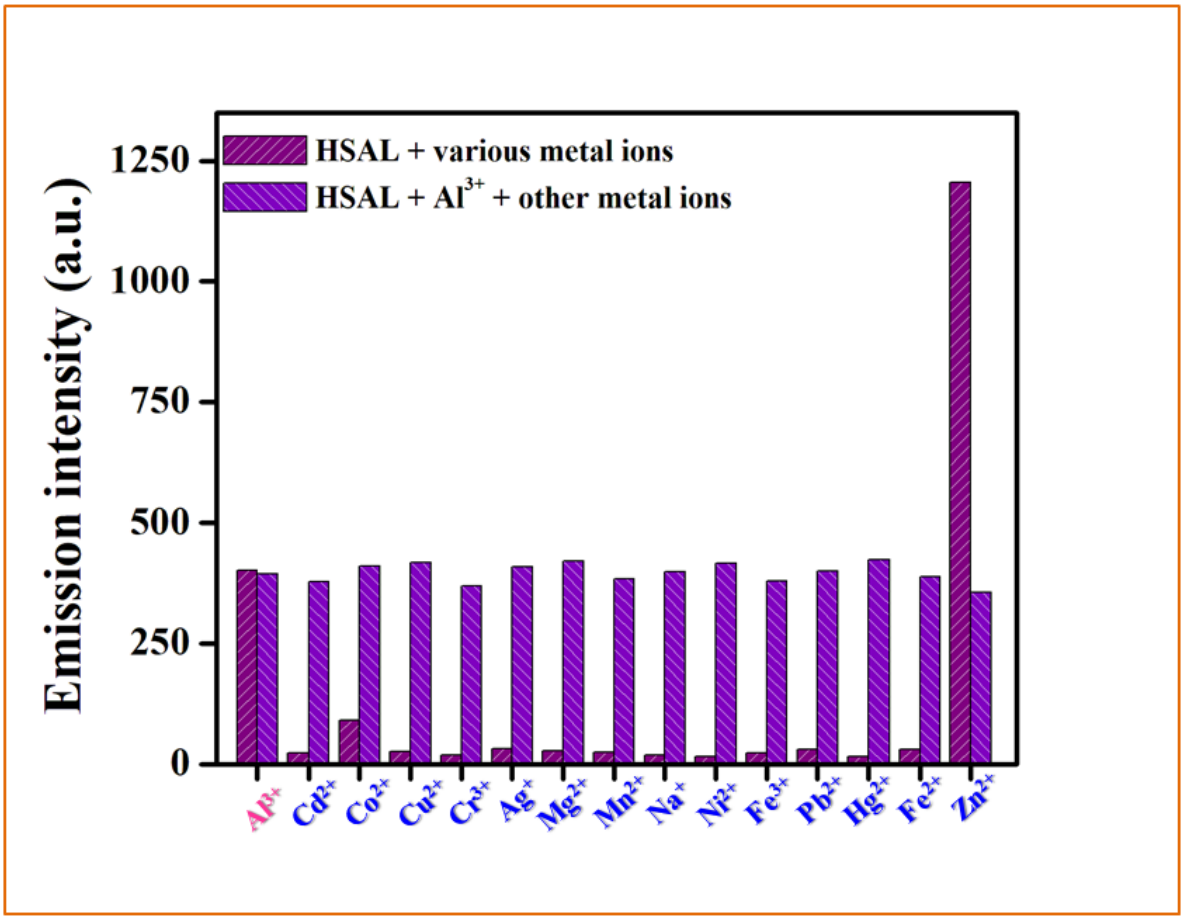

Fig S25. Competitive selectivity of **HSAL** towards the (A) Al^{3+} ions at λ= 440 nm in DMF-Tris HCl buffer solution (10 mM Tris HCl, 8:2 v/v, pH 7.4) (λ_{ex}= 355 nm).

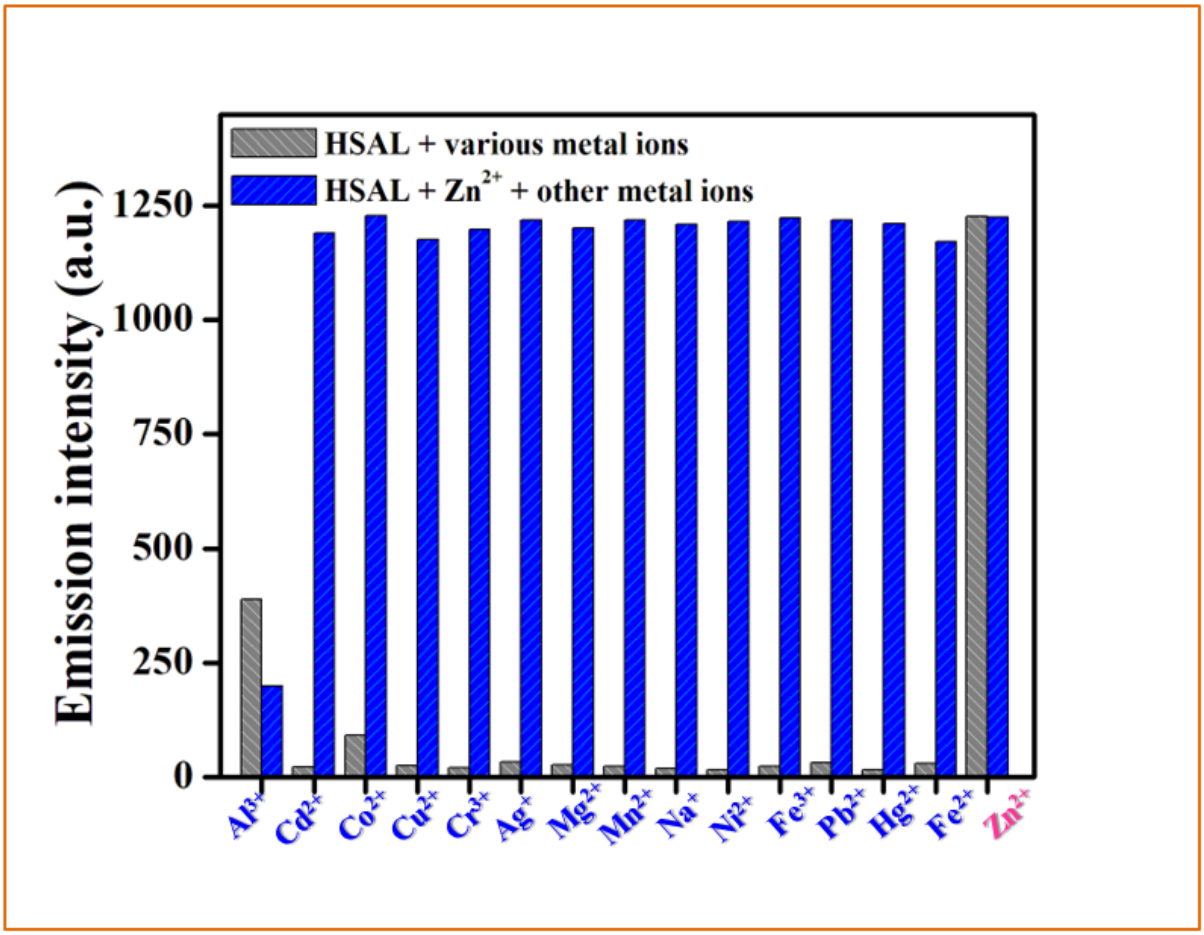

Fig S26. Competitive selectivity of **HSAL** towards the (A) Zn^{2+} ions at λ= 470 nm in DMF-Tris HCl buffer solution (10 mM Tris HCl, 8:2 v/v, pH 7.4) (λ_{ex}= 355 nm).

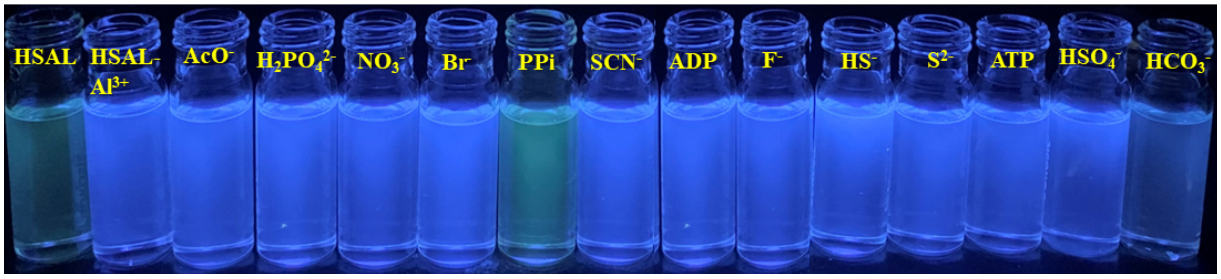

Fig S27. Photographic images of vials containing HSAL-Al^{3+} on adding different anions under UV light.

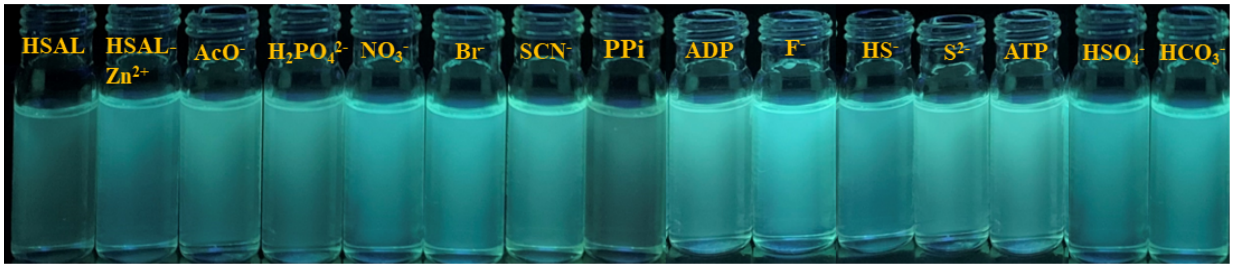

Fig S28. Photographic images of vials containing HSAL-Zn^{2+} on adding different anions under UV light.

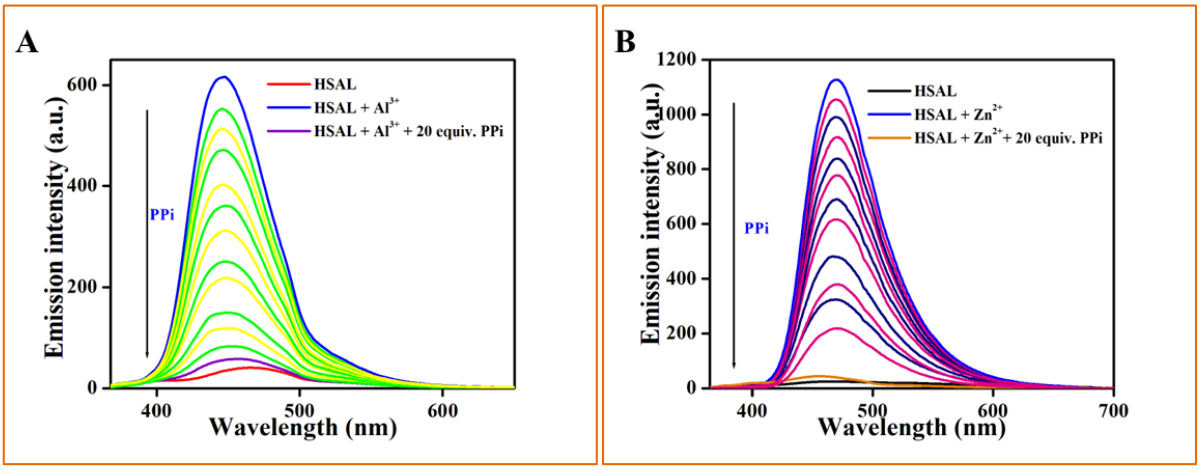

Fig S29. Emission titration spectra of (A) HSAL-Al^{3+} and (B) HSAL-Zn^{2+} ensembles on incremental addition of PPi in DMF-Tris HCl buffer solution (10 mM Tris HCl, 8:2 v/v, pH 7.4) (λ_{ex}= 355 nm).

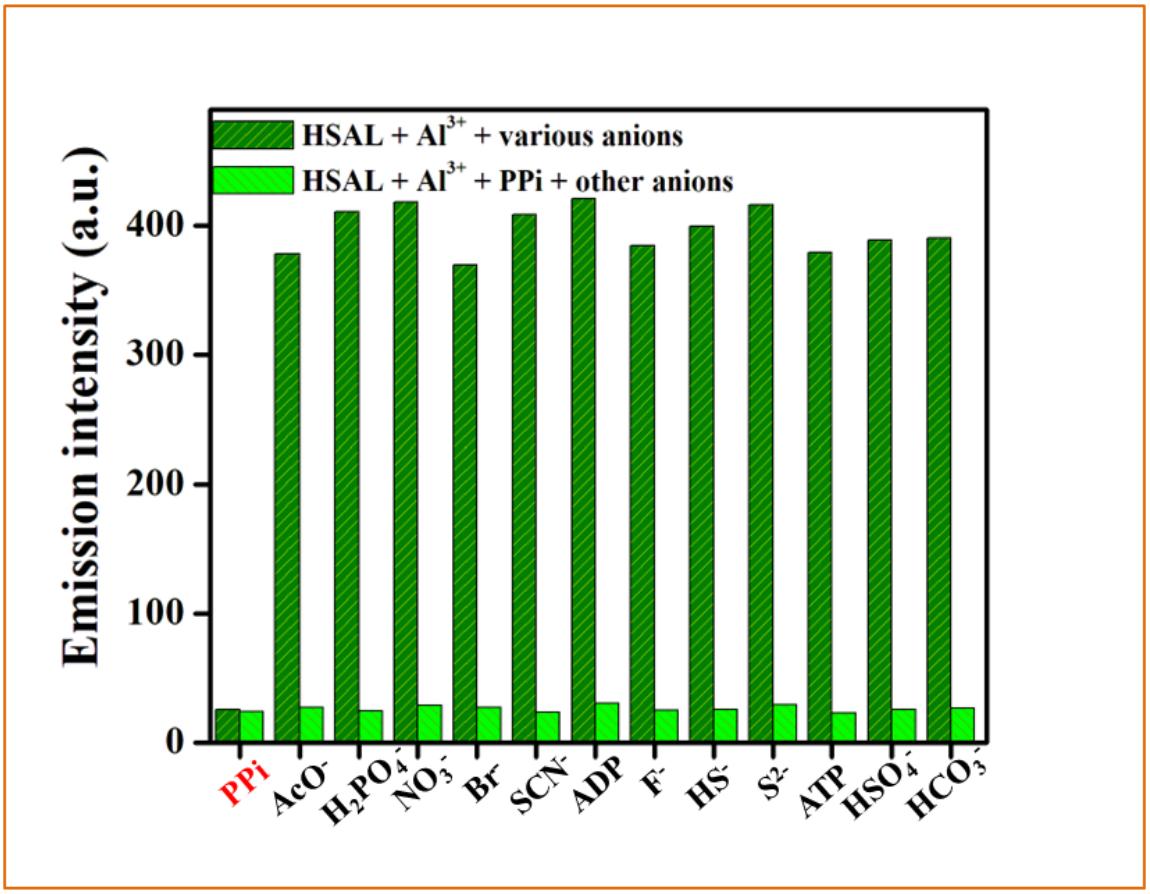

Fig S30. Selectivity graph of the HSAL–Al^{3+} ensemble with PPi in DMF-Tris HCl buffer solution (10 mM Tris HCl, 8:2 v/v, pH 7.4) (λ_{ex}= 355 nm).

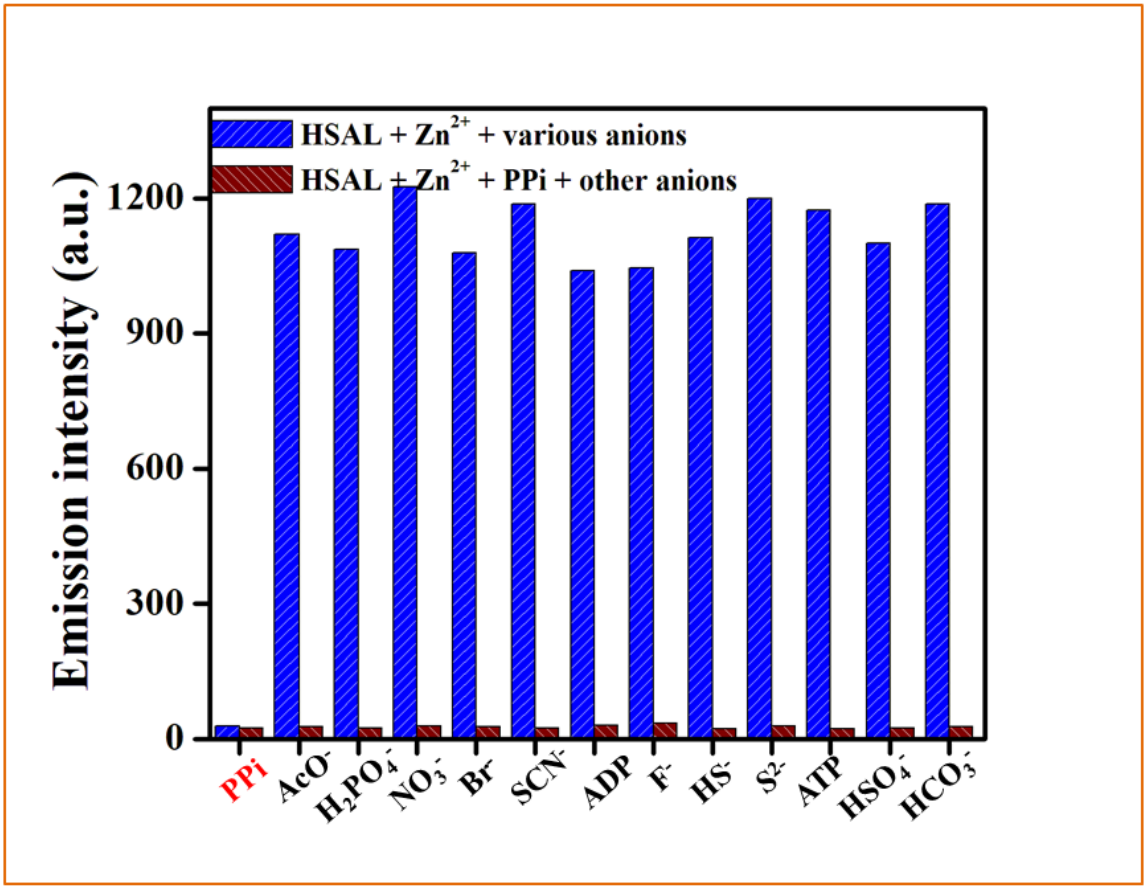

Fig S31. Selectivity graph of the HSAL – Zn^{2+} ensemble with PPi in DMF-Tris HCl buffer solution (10 mM Tris HCl, 8:2 v/v, pH 7.4) (λ_{ex}= 355 nm).

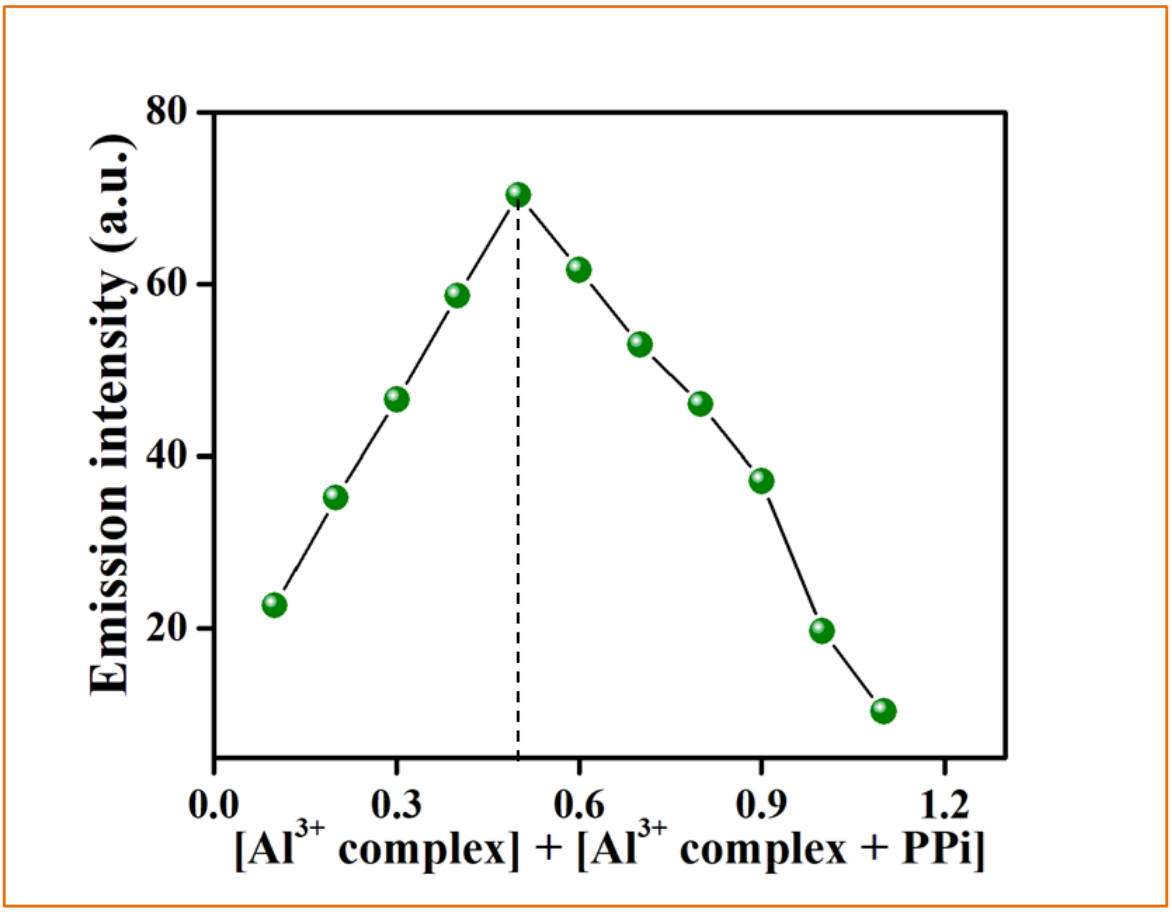

Fig S32. Job's plot of HSAL-Al^{3+} with PPi showing 1:1 binding stoichiometry.

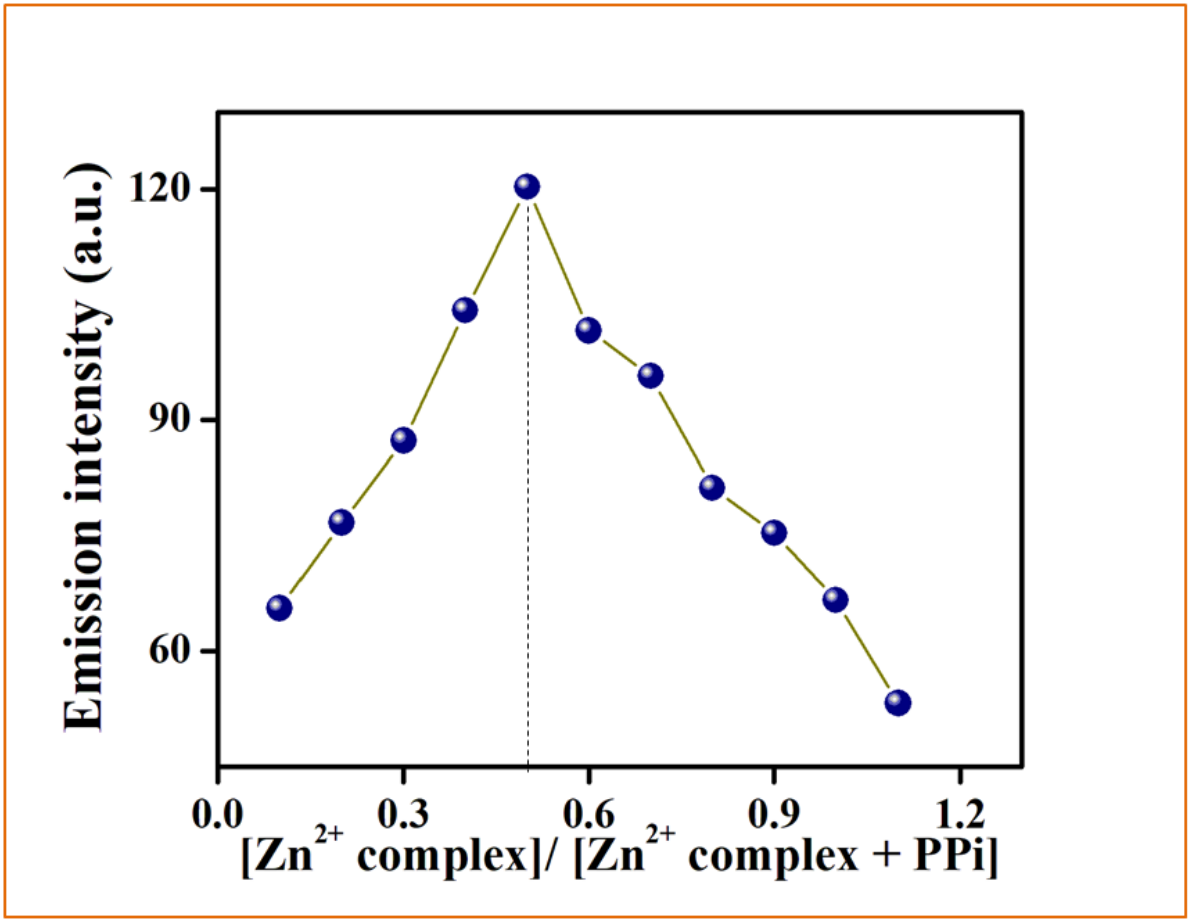

Fig S33. Job's plot of HSAL-Zn^{2+} with PPi showing 1:1 binding stoichiometry.

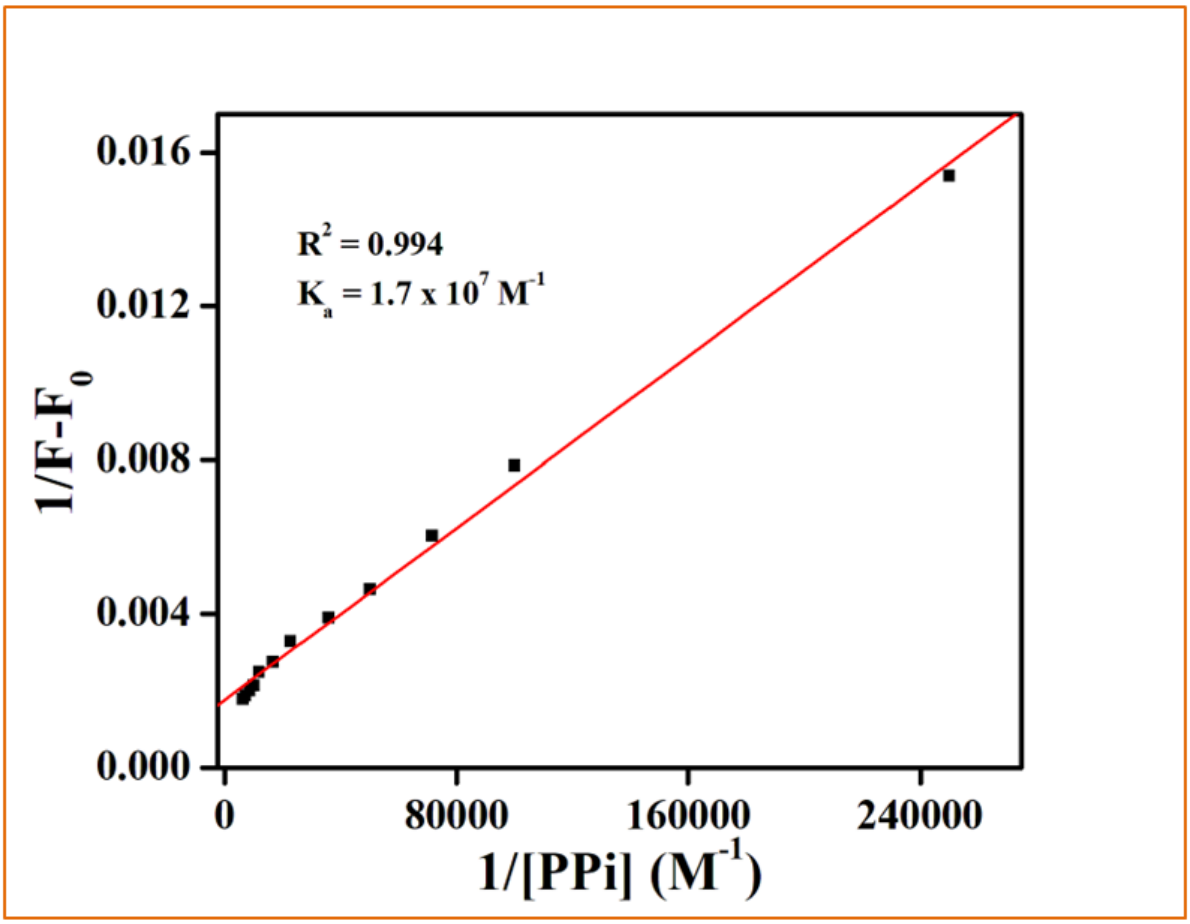

Fig. S34. Benesi-Hildebrand plot for the detection of PPi ion by HSAL-Al^{3+} ensemble.

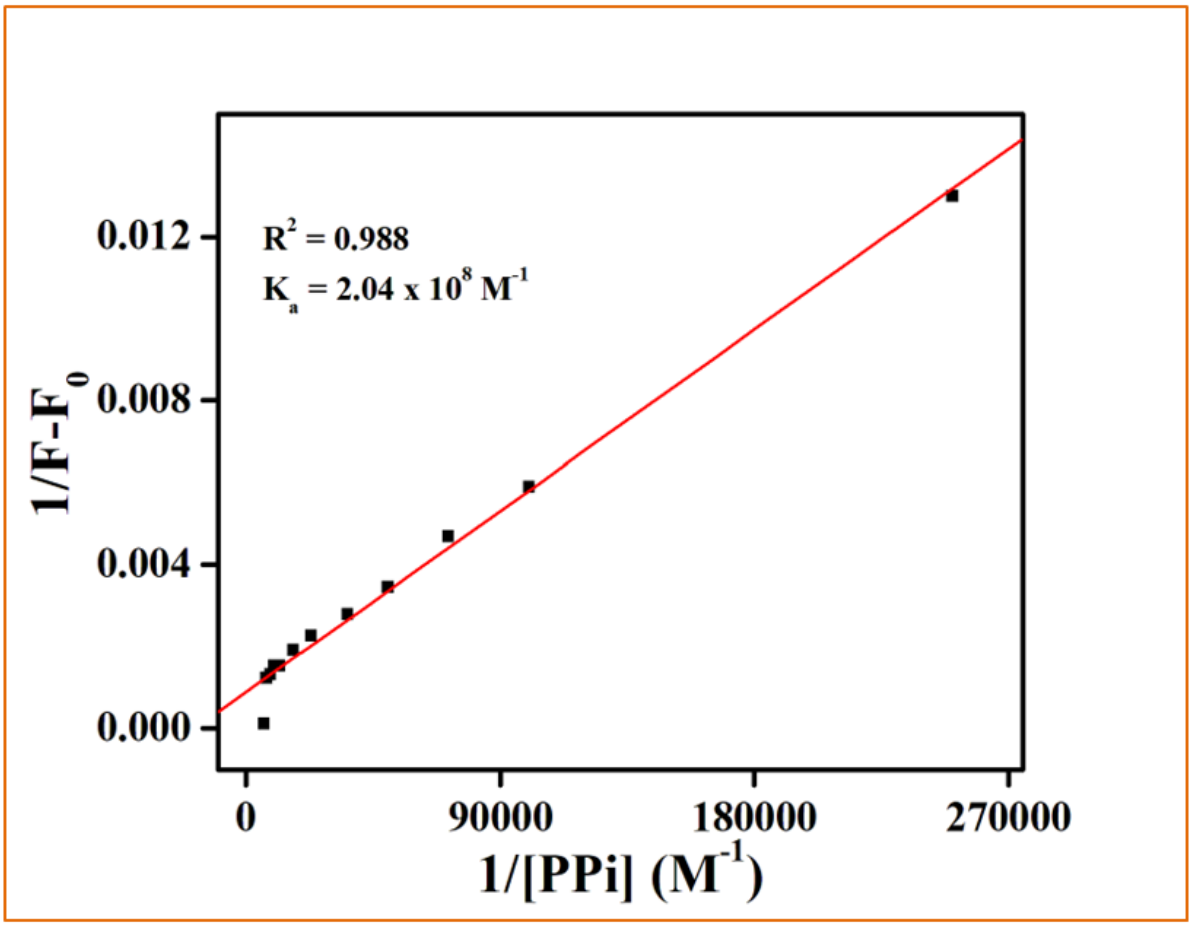

Fig. S35. Benesi-Hildebrand plot for the detection of PPi ion by HSAL-Zn^{2+} ensemble.

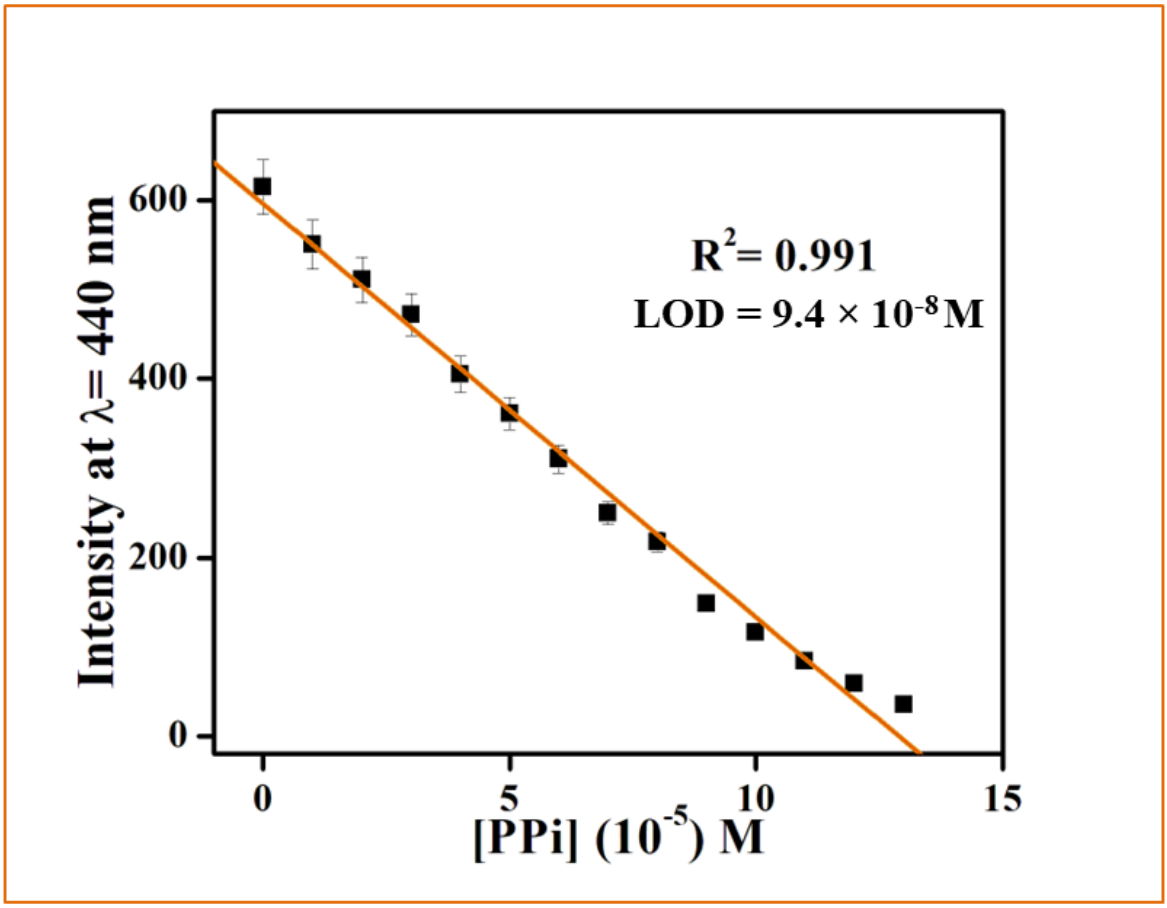

Fig. S36. Linear fit curve of HSAL-Al^{3+} with respect to PPi concentration at 440 nm. Standard deviations are represented by error bar (n=5).

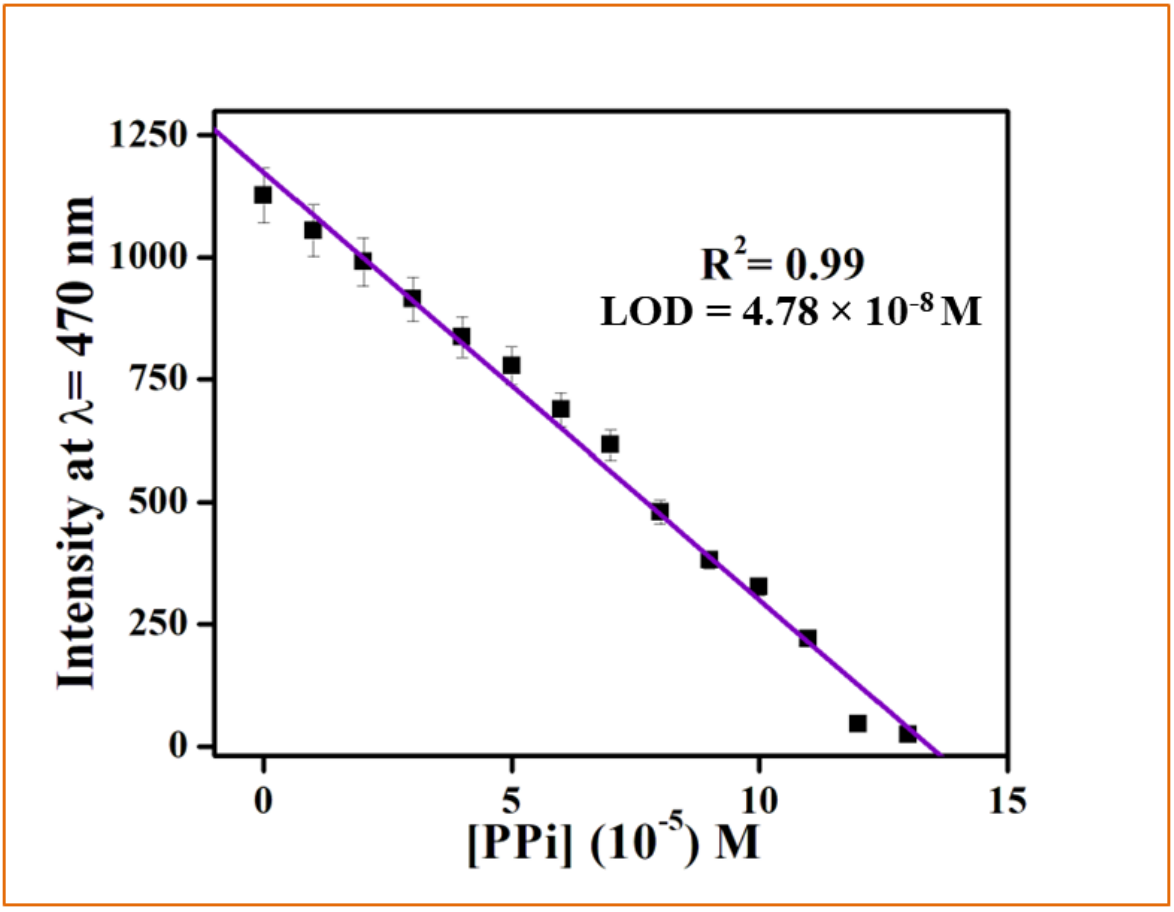

Fig. S37. Linear fit curve of HSAL-Zn^{2+} with respect to PPi concentration at 470 nm. Standard deviations are represented by error bar (n=5).

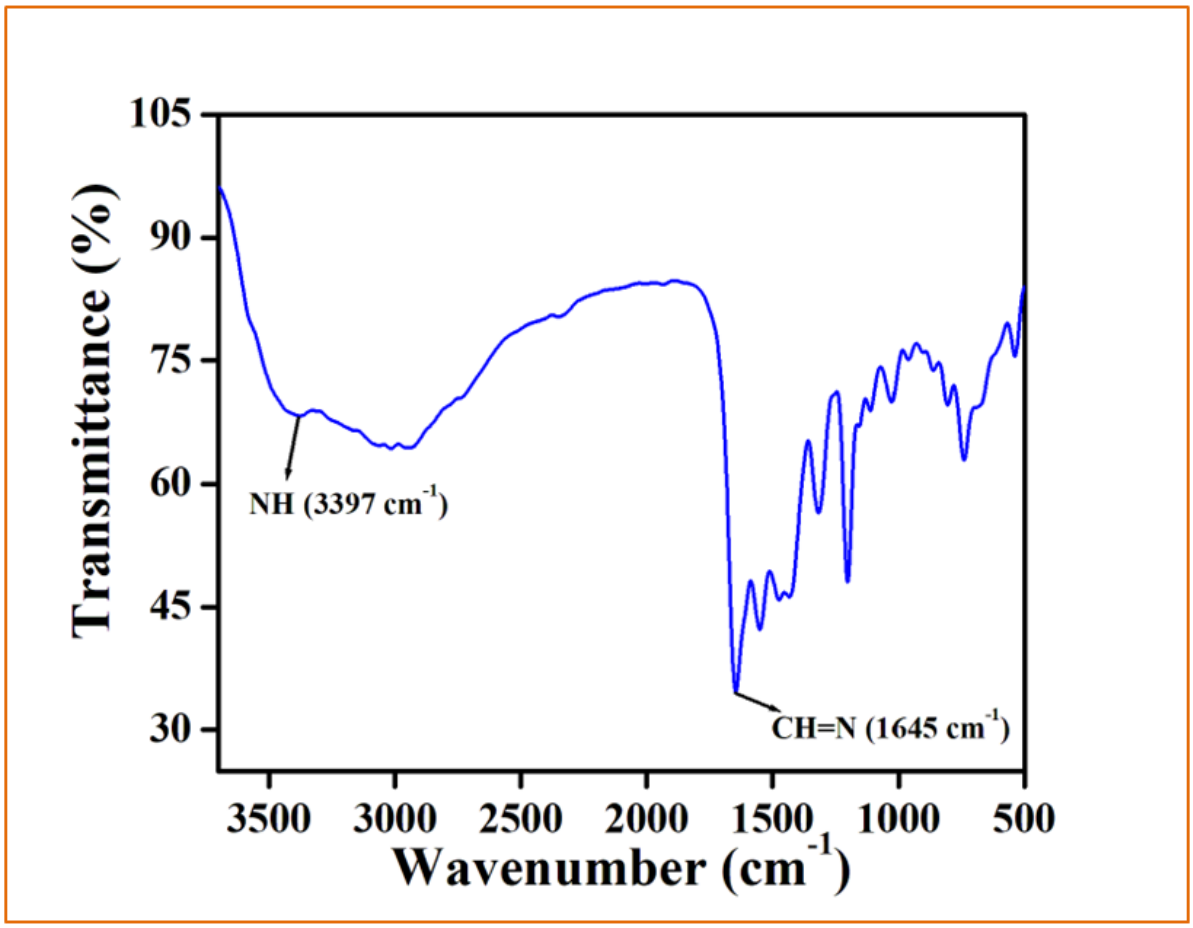

Fig S38. IR spectra of **HSAL**-Al^{3+} ensemble.

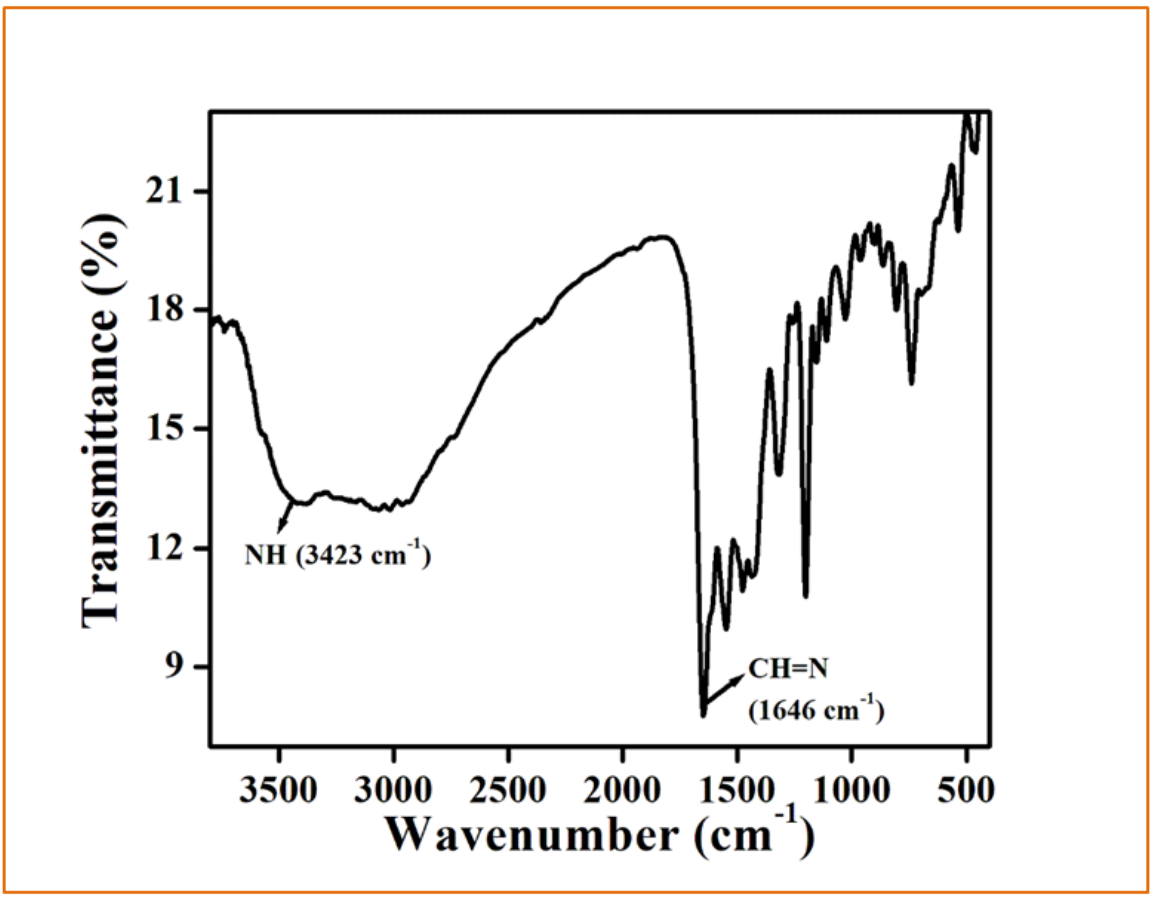

Fig S39. IR spectra of **HSAL**-Zn^{2+} ensemble.

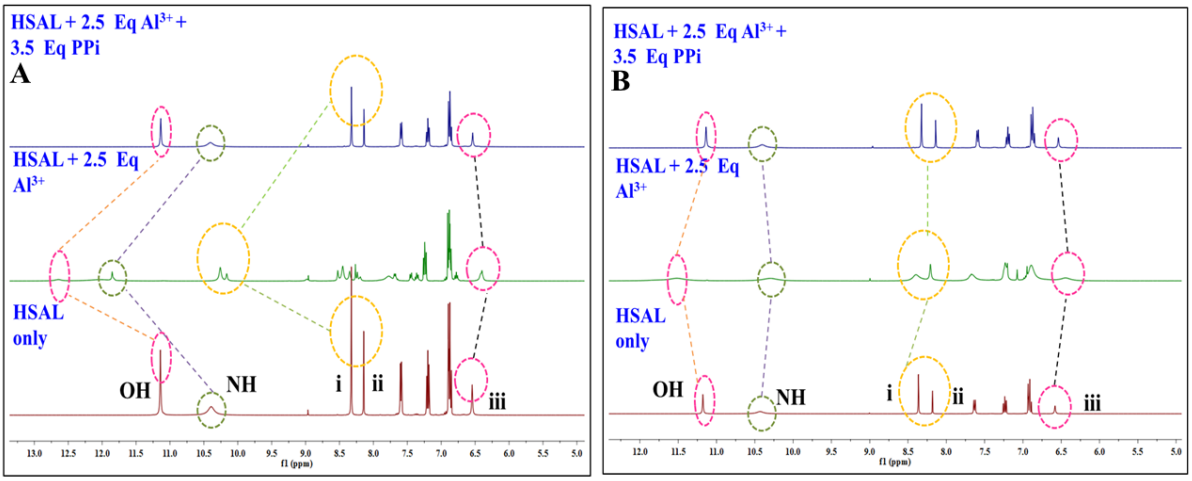

Fig S40. ^{1}H NMR spectra of **HSAL** in the range 5-12 ppm with 2.5 equiv. subsequent addition of (A) Al^{3+} and PPi, (B) Zn^{2+} and PPi in DMSO-d_6

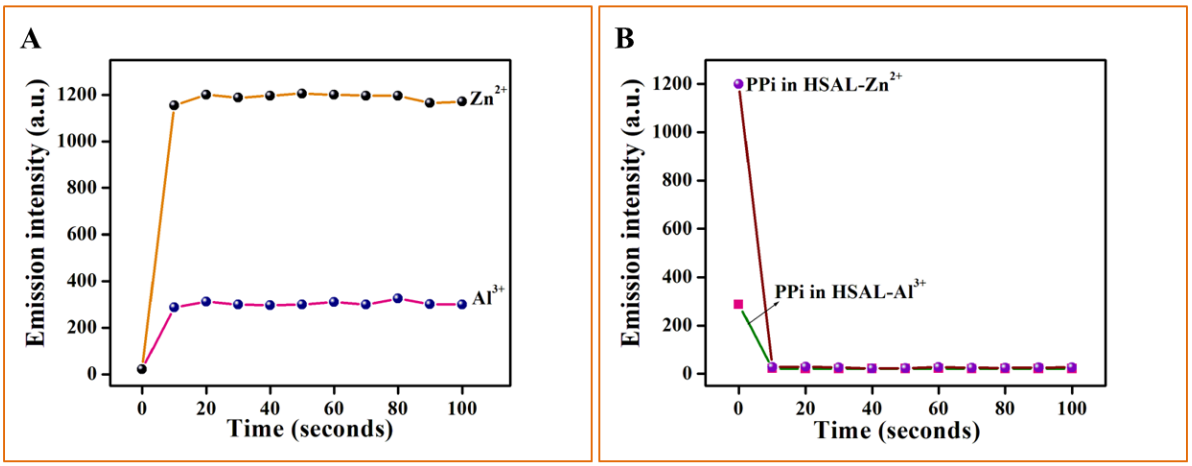

Fig S41. Emission response of (A) **HSAL** towards Al^{3+}/Zn^{2+} ions, (B) HSAL-Al^{3+} and HSAL-Zn^{2+} towards PPi with respect to time.

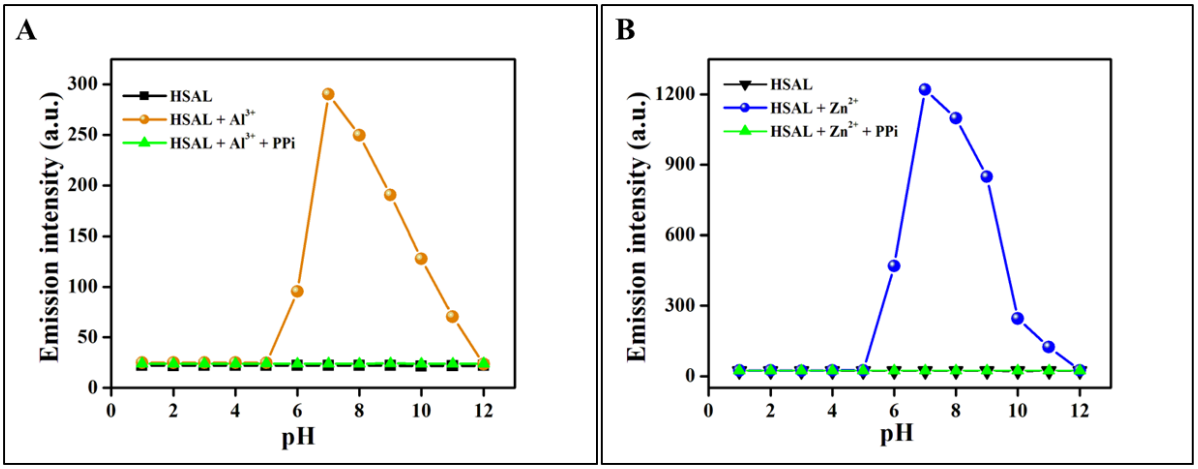

Fig S42. Effect of pH on the fluorescence intensity of **HSAL** (16 μM) in the absence of Al^{3+}/Zn^{2+} (black line), in the presence of Al^{3+}/Zn^{2+} ions and the effect of pH on the fluorescence intensity of HSAL-Al^{3+} and HSAL-Zn^{2+} ensembles in the presence of PPi.

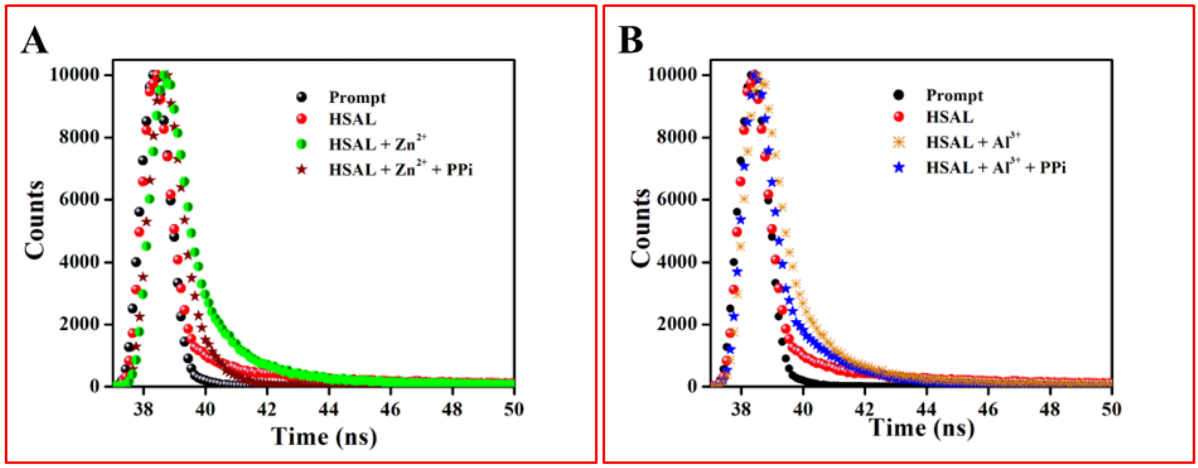

Fig S43. Time resolved photoluminescence spectra explaining the decay profiles of **HSAL** on adding (A) Al^{3+} and PPi, (B) Zn^{2+} and PPi.

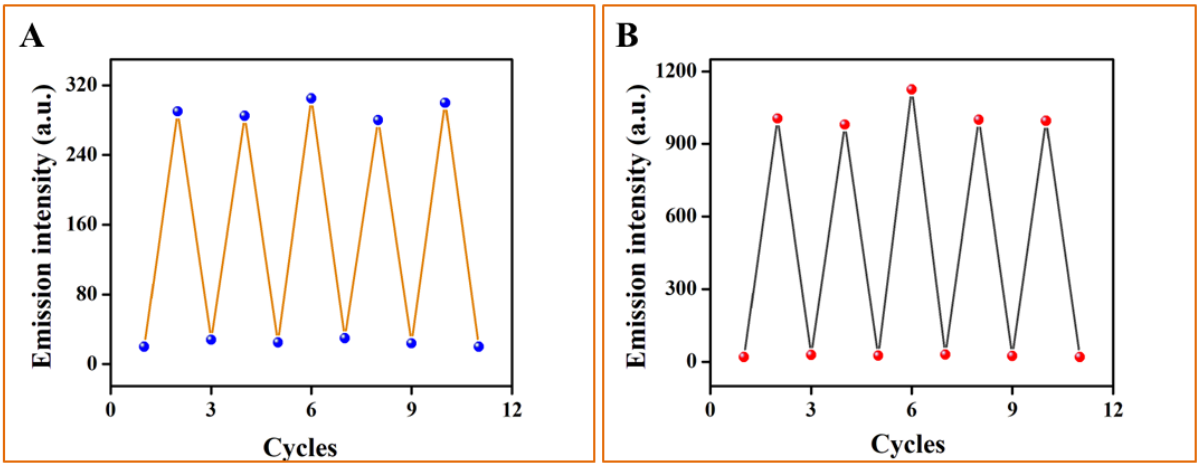

Fig S44. Reversible switching emission characteristics of **HSAL** at (A) 440 nm upon the alternate addition of Al^{3+} and PPi and (B) 470 nm upon the alternate addition of Zn^{2+} and PPi.

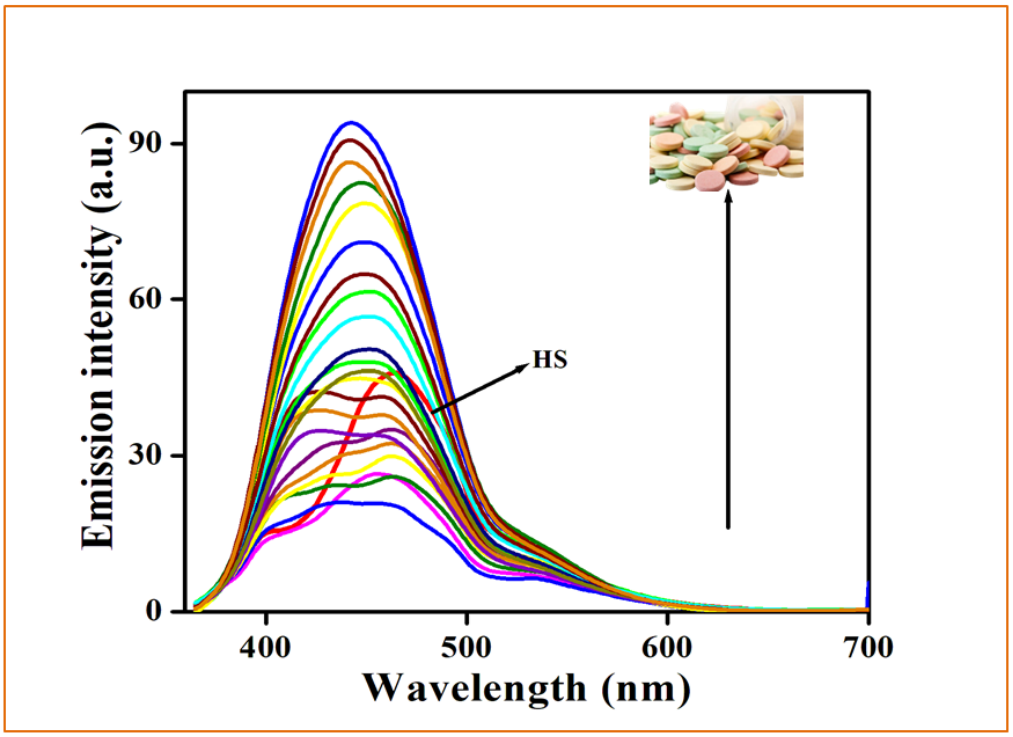

Fig S45. Emission spectral titration experiments of **HSAL** (20 μM, λ_{ex}= 355 nm) with aqueous extract (0 -130 μL) of Gelusil® antacid tablet in DMF–Tris–HCl buffer (10 mM Tris HCl, 8:2 v/v, pH 7.4).

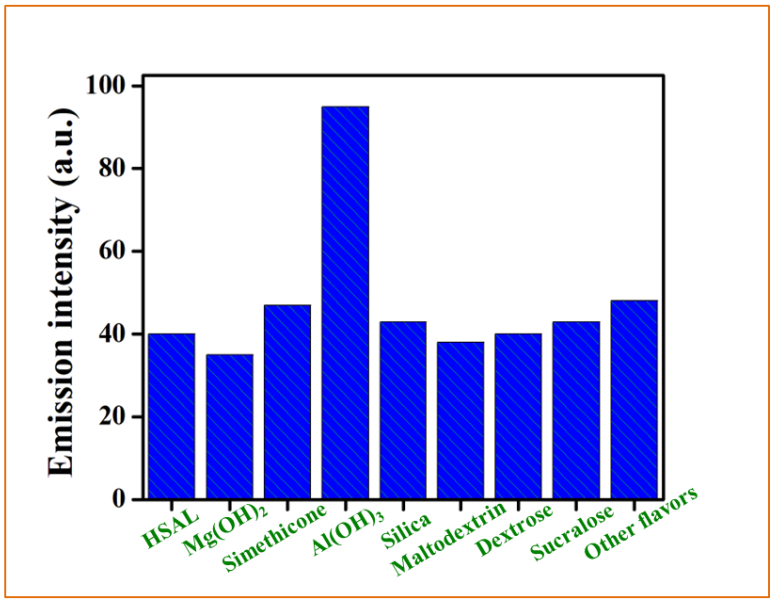

Fig S46. Changes in emission intensity of HSAL (20 μM), on adding 10 equiv. of different ingredients present in antacid tablets.

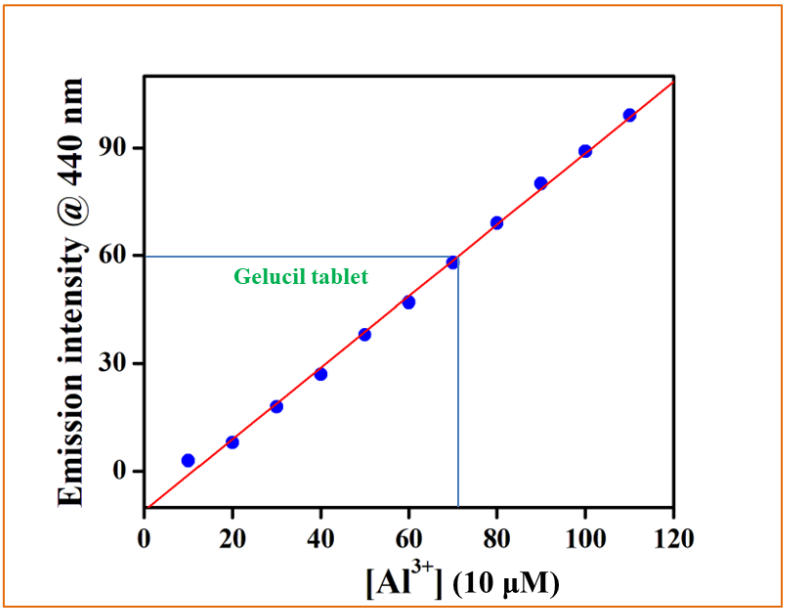

Fig S47. Emission titration curve for **HSAL** (20 μM) *vs* Al^{3+} ions (λ_{ex} = 355 nm) for the qualitative determination of Al^{3+} ions from Gelucil tablet extracts.

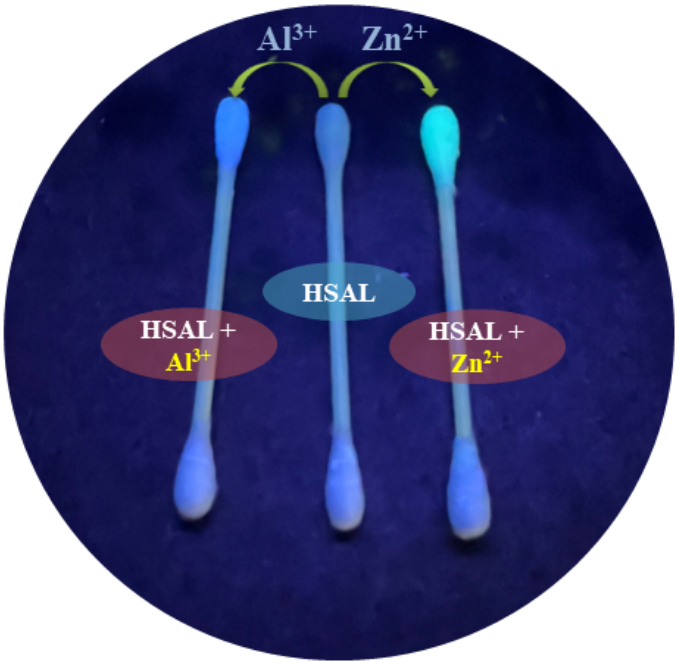

Fig S48. Cotton swabs dipped in solutions of **HSAL**, HSAL-Al^{3+} and HSAL-Zn^{2+}

Table S5. Performance comparison of recently published probes.

Sl. No.	Structure	Detection limit	Association constant	Applications	References
1	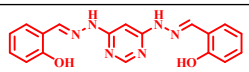	Al^{3+}: 5.48 nM Zn^{2+}: 9.28 nM	Al^{3+}: 0.14 × 10^8 M^{-1} Zn^{2+}: 0.13 × 10^7 M^{-1}	• Logic gate • Molecular keypad lock • Thin-film • Tablets • Real water • Cotton swabs	*This work*
2	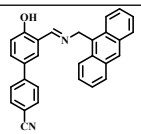	Al^{3+}: 5.22 × 10^{-8} M Zn^{2+}:7.88 × 10^{-8} M	Al^{3+}:6.24 Zn^{2+}:2.81 (log K_a)	• Off-on fluorescent sensor. • Test paper strip	https://doi.org/10.1016/j.snb.2018.06.019[6]
3	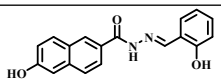	Al^{3+}: 7.55 × 10^{-8} M Zn^{2+}: 3.02 × 10^{-7} M	Al^{3+}: 4.45 × 10^5 M^{-1} Zn^{2+}: 8.48 × $10^4 M^{-1}$	• Real water samples analysis. • Test paper. • Logic gates representation. • Imaging in plant.	https://doi.org/10.1016/j.saa.2019.117786[7]
4	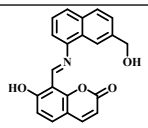	Al^{3+}:1.14 × 10^{-8} M Zn^{2+}: 3.75 × 10^{-8}M	Al^{3+}: 5.28 × 10^5 M^{-1} Zn^{2+}: 1.27 × 10^5 M^{-1}	• Determination of Zn^{2+} and Al^{3+} in filter paper. • pH studies • Fluorescence imaging in living cells.	https://doi.org/10.1016/j.saa.2019.117493[8]
5	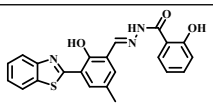	Al^{3+}: 1.42×10^{-7} M Zn^{2+}: 1.27×10^{-7} M	Al^{3+}: 2.79×10^2 $M^{-1/2}$ Zn^{2+}: 3.19×10^4 M^{-1}	• Real water samples. • Test strips.	https://doi.org/10.1016/j.molliq.2019.112250[9]
6	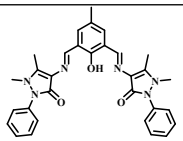	Al^{3+}:3.0 ×10^{-8} M Zn^{2+}:2.1×10^{-8} M	Al^{3+}: 7.63 × 10^4 M^{-1} Zn^{2+}: 3.42 × 10^4 M^{-1}	• TLC Strips.	10.1039/C9PP00226J[10]
7	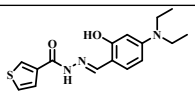	Al^{3+}: 3.7 × 10^{-9} M Zn^{2+}: 3.0 ×	Al^{3+}: 1.16 ×$10^4 M^{-1}$ Zn^{2+}: 2.08	• Turn on sensor. • Real sample	https://doi.org/10.1016/j.aca.2018.10.043[11]

		10^{-8} M	$\times 10^{4} M^{-1}$	analysis. • Cell imaging.	
8	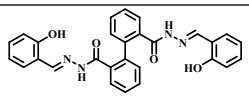	Al^{3+}: 4.2×10^{-8} M Zn^{2+}:3.4×10^{-8} M	Al^{3+}: $2.43 \times 10^{8} M^{-2}$ Zn^{2+}:$2.08\times 10^{7} M^{-2}$	• Real sample analysis. • Molecular logic gate. • Test kits.	10.1039/d2nj03144b[12]
9	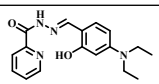	Al^{3+}: 8.30×10^{-8} M Zn^{2+}: 1.24×10^{-7} M	Al^{3+}: $1.3 \times 10^{6} M^{-1}$ Zn^{2+}: $7.9 \times 10^{4} M^{-1}$	• Cytotoxicity and cell imaging. • Logic gate.	10.1039/C8TB01743C[13]
10	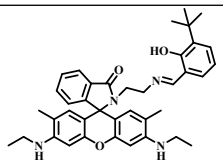	Al^{3+}:1.098×10^{-8}M Zn^{2+}: 7.692×10^{-8}M	Al^{3+}: $9.38 \times 10^{3} M^{-1}$ Zn^{2+}: $4.75 \times 10^{4} M^{-1}$	• Reversibility Test. • Naked Eye Detection. • Cell Imaging Studies.	10.1021/acsomega.9b00475[14]

References

1. A. S. Meyer Jr and G. H. Ayres, *Journal of the American Chemical Society*, 1957, **79**, 49-53.
2. C. R. Lohani, J.-M. Kim, S.-Y. Chung, J. Yoon and K.-H. Lee, *Analyst*, 2010, **135**, 2079-2084.
3. H. A. Benesi and J. Hildebrand, *Journal of the American Chemical Society*, 1949, **71**, 2703-2707.
4. T. Thiruppathiraja, A. L. Arokiyanathan and S. Lakshmipathi, *Fuel Cells*, 2021, **21**, 490-501.
5. T. Thiruppathiraja and S. Lakshmipathi, *Applied Physics A*, 2023, **129**, 218.
6. S. Erdemir and O. Kocyigit, *Sensors and Actuators B: Chemical*, 2018, **273**, 56-61.
7. X.-J. Sun, T.-T. Liu, N.-N. Li, S. Zeng and Z.-Y. Xing, *Spectrochimica Acta Part A: Molecular and Biomolecular Spectroscopy*, 2020, **228**, 117786.
8. J. Fu, Y. Chang, B. Li, X. Wang, X. Xie and K. Xu, *Spectrochimica Acta Part A: Molecular and Biomolecular Spectroscopy*, 2020, **225**, 117493.
9. T.-T. Liu, J. Xu, C.-g. Liu, S. Zeng, Z.-Y. Xing, X.-J. Sun and J.-L. Li, *Journal of Molecular Liquids*, 2020, **300**, 112250.
10. S. Dey, A. Maity, M. Shyamal, D. Das, S. Maity, P. K. Giri, N. Mudi, S. S. Samanta, P. Hazra and A. Misra, *Photochemical & Photobiological Sciences*, 2019, **18**, 2717-2729.
11. Y. Li, Q. Niu, T. Wei and T. Li, *Analytica Chimica Acta*, 2019, **1049**, 196-212.
12. A. Hoque, M. S. Islam, M. A. Khan, S. Ghosh, M. A. Sekh, S. Hussain and M. A. Alam, *New Journal of Chemistry*, 2022, **46**, 16025-16034.
13. H. Liu, T. Liu, J. Li, Y. Zhang, J. Li, J. Song, J. Qu and W.-Y. Wong, *Journal of Materials Chemistry B*, 2018, **6**, 5435-5442.
14. A. Roy, U. Shee, A. Mukherjee, S. K. Mandal and P. Roy, *ACS Omega*, 2019, **4**, 6864-6875.